

Fast-ParC: Position Aware Global Kernel for ConvNets and ViTs

Tao Yang, Haokui Zhang, Wenzhe Hu, Changwen Chen, *Fellow, IEEE*, Xiaoyu Wang

Abstract—Transformer models have made tremendous progress in various fields in recent years. In the field of computer vision, vision transformers (ViTs) also become strong alternatives to convolutional neural networks (ConvNets), yet they have not been able to replace ConvNets since both have their own merits. For instance, ViTs are good at extracting global features with attention mechanisms while ConvNets are more efficient in modeling local relationships due to their strong inductive bias. A natural idea that arises is to combine the strengths of both ConvNets and ViTs to design new structures. In this paper, we propose a new basic neural network operator named position-aware circular convolution (ParC) and its accelerated version Fast-ParC. The ParC operator can capture global features by using a global kernel and circular convolution while keeping location sensitiveness by employing position embeddings. Our Fast-ParC further reduces the $\mathcal{O}(n^2)$ time complexity of ParC to $\mathcal{O}(n \log n)$ using Fast Fourier Transform. This acceleration makes it possible to use global convolution in the early stages of models with large feature maps, yet still maintains the overall computational cost comparable with using 3×3 or 7×7 kernels. The proposed operation can be used in a plug-and-play manner to 1) convert ViTs to pure-ConvNet architecture to enjoy wider hardware support and achieve higher inference speed; 2) replacing traditional convolutions in the deep stage of ConvNets to improve accuracy by enlarging the effective receptive field. Experiment results show that our ParC op can effectively enlarge the receptive field of traditional ConvNets, and adopting the proposed op benefits both ViTs and ConvNet models on all three popular vision tasks, image classification, object detection, and semantic segmentation. Source code will be available at https://github.com/yangtao2019yt/Fast_ParC.git.

Index Terms—global receptive field, position aware circular convolution, positional embedding, pure convolution operation, Fast Fourier Transform

1 INTRODUCTION

VISION transformer has been a rising in recent years. Transformer was firstly proposed in 2017 to solve the NLP task [2]. In 2020, Dosovitskiy et al. [3] directly applied the original transformer to image classification task and found it achieved better results than convolutional networks (ConvNets), when pretrained on large datasets (e.g. ImageNet-21K or JFM-300M [4]). ViT and its variants are then widely used on other downstream vision tasks such as object detection [5] [6], semantic segmentation [7], and multi-modal tasks like human object interactions (HOI) [8], text-to-image (T2I) synthesis [9], etc.. Despite the great success of transformers, they still cannot replace ConvNets completely. As is summarized in previous works [1] [10] [11] [12], when compared with ViTs, ConvNets have better hardware support and are easier to train. In addition, ConvNets still dominate in the domain of lightweight models [13] [14] for mobile and other edge computing scenarios.

Both transformers and ConvNets have their distinct features. For transformers, the widely recognized multi-head attention mechanism is designed to capture long range pair-wise relationships between tokens, which provides

transformers with powerful global modeling ability. While empowered by this representation capability, it however requires higher computation budget as well. The time complexity for self-attention is quadratic over the number of tokens, and hence slow to process high resolution feature maps. Different from it, convolution operation excel at extracting local information. It captures the local information within a small sliding-window, usually 3×3 , and reuses the same convolution kernel for different inputs and different spatial positions. It can be interpreted as an effective implicit weight sharing scheme, making the required parameters of the convolution grows only linearly with the input. Furthermore, ConvNets have been well studied and used for much longer time, so they enjoy some other unique advantages as well. For example, compression algorithms like pruning [17] and quantization [18] for ConvNets are mature. As for hardware implementations, there are also many existing acceleration schemes (e.g. Winograd [19], FFT [20], im2col [21]) whether on general platforms like CPU, GPU or dedicated accelerators like FPGA, ASIC. In a word, convolution operation is cheaper in implementation, but it cannot capture global relationship like self-attention does. Clearly, these exist a complementary relationship between transformers' representation ability and ConvNets' efficiency, both of which are indispensable for practical applications.

There are some recent works to combine the merits of transformers and ConvNets. PVT [22], Swin [23] and CoAtNet [24] attempt to reintroduce inductive bias of convolution (such as its sliding-window strategy), to help transformer models to learn better. Works like LeViT [25],

• Haokui Zhang, Wenzhe Hu and Xiaoyu Wang are with Intellifusion, Shenzhen, China, 518000.

• Tao Yang and Changwen Chen are with CHEN Lab, Department of Computing, Hong Kong Polytechnic University, Hong Kong, China, 999077.

• Work done during an internship at Intellifusion. A preliminary version [1] of this work has been presented in the ECCV 2022

Manuscript received xxxx, xxxx;

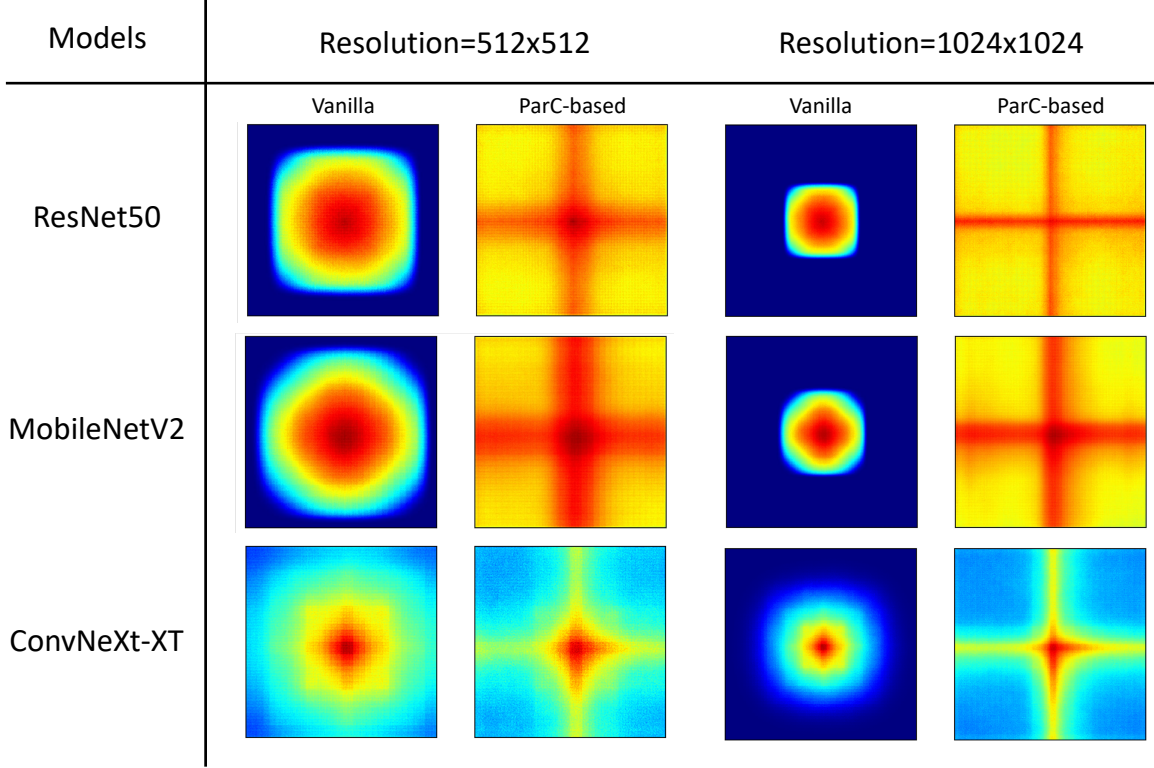


Fig. 1: Visualization of the Effective Receptive Field(ERF) [15] of different convolutional neural networks(CNNs). ParC significantly increase the CNNs' ERF to global. Code are based on the repository pulished by RepLKNet [16].

MobileViT [11], EfficientFormer [26] focus on designing efficient hybrid architectures. Most of these works bring the two kind of networks together, but they fail to tackle the key problem: the extra computational and engineering complexity of the newly introduced attention operator. It's natural to ask: if it is possible to design a new operator different from self-attention and traditional convolution, that has the advantages of both sides simultaneously?

In this paper, we construct such a new plug-and-play operator named ParC, combining the merits of both transformers and ConvNets. ParC has a global receptive field, since we use global kernels ($K_h = H$ or $K_w = W$) and adopt circular convolution scheme. We then adopt a explicit learnable positional embedding before convolution to keep our model positional sensitive. As shown in Fig. 1, different ConvNet models improve their effective receptive fields to global by simply applying the proposed ParC operator. As ParC uses pure convolution operation, it is efficient to be deployed on different platforms. Lastly, we take apart 2D convolution into two 1D convolution to overcome the increase in FLOPs/parameters. Based on the above design, we achieve the goal of extracting global feature, while still keeping a low cost in terms of space and time complexity. Through experiments, we verify the effectiveness of the new operator in a wide range of tasks and models. In short, the contribution of this paper can be summarized as the following three points:

- 1) An effective new operator ParC is proposed, combining the merits of both ViTs and ConvNets. Experiments demonstrated the advantages of ParC by applying it

to a wide ranges of models, including MobileViT [27], ResNet50 [28], MobileNetV2 [14] and ConvNext [27]. We also evaluate these models on multiple tasks, including classification, detection and segmentation.

- 2) Fast-ParC is proposed to overcome the problem that the complexity of ParC become overwhelming when the resolution of input feature is large. Fast-ParC is theoretically equivalent to ParC, e.g. their outputs are identical when given the same input. However it is far more efficient than ParC when given a large resolution (e.g. 112×122). Fast-ParC extends the usage scenarios of ParC, making it a more widely applicable operator.
- 3) The internal mechanism of the new operator is analyzed. By visualization, we show several distinct differences between ParC and vanilla convolution. We show that the effective receptive field (ERF) [15] of vanilla ConvNet is very limited, while the ParC-based Network has a global ERF indeed. We also show by Grad-CAM [29] that ParC-based networks are more comprehensive than vanilla ConvNets in focusing on the important regions of images. We also provide detailed analysis over the difference between ParC and vanilla convolution.

2 RELATER WORK

2.1 Theoretical/Effective Receptive Field

Hebel et al. [30] found in neuroscience that the neurons in the shallow layer extracts local features only, and the scope covered are accumulated layer by layer, called the "receptive field (RF)". Since the success of VGGNet [31],

the design of CNN architecture follow a similar pattern [28] [32] [14] [13] - using a stacking of small kernels like 3×3 instead of larger kernels. Some previous work give the theoretical computation of CNN's receptive field [33] [34], namely theoretical receptive field (TRF) - under which concept, the receptive field of two layers of 3×3 equals one layer of 5×5 . Nevertheless, some works [15] [34] cast doubt on this view, since in fact the importance of pixel degraded quickly from the center to the edge in a feature map. Later, the effective receptive field (ERF) was proposed to measure the region of input image which could actually impact the neurons' activation pattern. Luo et al. [15] back-propagate the center pixel and compute the partial derivative of input image to examine this region. And by studying a sequence of convolution networks, they found the effective receptive field is usually much smaller than their theoretical counterparts. SKNet [35] adopts attention mechanisms in selecting appropriate receptive field. RF-Next [36] proposes a NAS-based workflow to search the receptive fields for models automatically. These works show that a proper decision of receptive field could be quite beneficial for networks' performance. Recent work also found that enlarging the receptive field of convolution network can lead to better model performance. We call them "Large Kernel Convolution Network", which will be discussed later in Section 2.3.

2.2 Vision Transformer and Hybrid Structures

ViTs achieves impressive performance on various vision tasks. However, the original ViT [3] has some restrictions. For instance, it is heavy weight, has low computational efficiency and is hard to train. Subsequent variants of ViTs are proposed to overcome these problems. From the point of improving training strategy, Touvron et al. [37] proposed to use knowledge distillation to train ViT models, and achieved competitive accuracy with less pre-training data. To further improve the model architecture, some researchers attempted to optimize ViTs by learning from ConvNets. Among them, PVT [22] and CVT [38] insert convolutional operations into each stage of ViT to reduce the number of tokens, and build hierarchical multi-stage structures. Swin transformer [23] computes self attention within shifted local windows. PiT [39] jointly use pooling layer and depth wise convolution layer to achieve channel multiplication and spatial reduction. CCNet [40] propose a simplified version of self attention mechanism called criss-cross attention and inserts it into ConvNets to build ConvNets with global receptive field. These papers clearly show that some techniques of ConvNets can be applied on vision transformers to design better vision transformer models.

Another popular line of research is combining elements of ViTs and ConvNets to design new backbones. Graham et al. mixed ConvNet and transformer in their LeViT [25] model, which significantly outperforms previous ConvNet and ViT models with respect to the speed/accuracy trade-off. BoTNet [41] replaces the standard convolution with multi-head attention in the last few blocks of ResNet. ViT-C [42] adds early convolutional stems to vanilla ViT. ConViT [43] incorporates soft convolutional inductive biases via a gated positional self-attention. The CMT [10] block consists of depth wise convolution based local perception unit and

a light-weight transformer module. CoatNet [24] merges convolution and self-attention to design a new transformer module, which focuses on both local and global information.

2.3 Large Kernel Convolution Network

Early ConvNets such as AlexNet [44] and GoogleNet [45] uses big kernel like 5×5 or 7×7 . But since the success of VGGNet [31], stacking small kernels like 3×3 and 1×1 becomes believed to be an efficient choice for computation and storage. Recently, inspired by the success of vision transformers, big kernels are reused as a powerful tool for improving model's performance again. ConvNext [27] modernizes a standard ResNet towards the design of a vision transformer by introducing a series of incremental but effective designs, where 7×7 depth-wise convolution is used following the spirit of windowed-SA in Swin [23]. RepLKNet [16] scales up convolution kernel to 31×31 and obtain a performance gain, but the re-parameterization trick used would burden the training process, and an extra conversion step is needed for model deployment. Later, Rao et al. use an even larger kernel of 51×51 with dynamic sparsity [46]. GFNet [47] replaces the SA (self-attention) in transformer blocks with a global Fourier convolution, implemented with FFT.

Our work is most closely related to RepLKNet [16] and GFNet [47]. Both these methods and our proposed ParC focus on enlarging the effective receptive field, but our proposed op is different from the following perspectives: 1) Our ParC uses learnable position embeddings to keep the result feature map position sensitive. This is important for location sensitive tasks such as semantic segmentation and object detection. Experiments in ablation study also verify this point. 2) Our ParC adopts light weight designs. RepLKNet use heavy 2D convolution kernels, and GFNet use a learnable complex weight matrix with shape $2CHW$, while ours uses two one dimensional convolutions, reducing the kernels to CH or CW . 3) Different from RepLKNet and GFNet which emphasis network designs holistically, our proposed ParC is a new basic operator, which can be inserted into ViTs and ConvNets in a plug-and-play manner. Our experimental results in Section 4.1 and 4.2 verifies this point. In addition, we also propose Fast-ParC, which further broaden the usage scenario of ParC.

3 THE PROPOSED FAST-PARC OPERATOR

In this section, we first introduce the proposed ParC operator by comparing it with the vanilla convolution operator. Then, we present the FFT accelerated version of ParC, named Fast-ParC. Finally, we explain how to use the proposed ParC in ViT and ConvNet models.

3.1 ParC Operation

3.1.1 Vanilla Depth-wise Convolution

To describe an 1D depth-wise convolution conducted in horizontal dimension (noted as Conv1d-H) on a 4D input tensor shaped as $B \times C \times H \times W$, we could firstly focus on one specific channel. We denote the output as $\mathbf{y} = \{y_1, \dots, y_{H-1}\}$, input as $\mathbf{x} = \{x_0, x_1, \dots, x_{H-1}\}$, the convolution weight

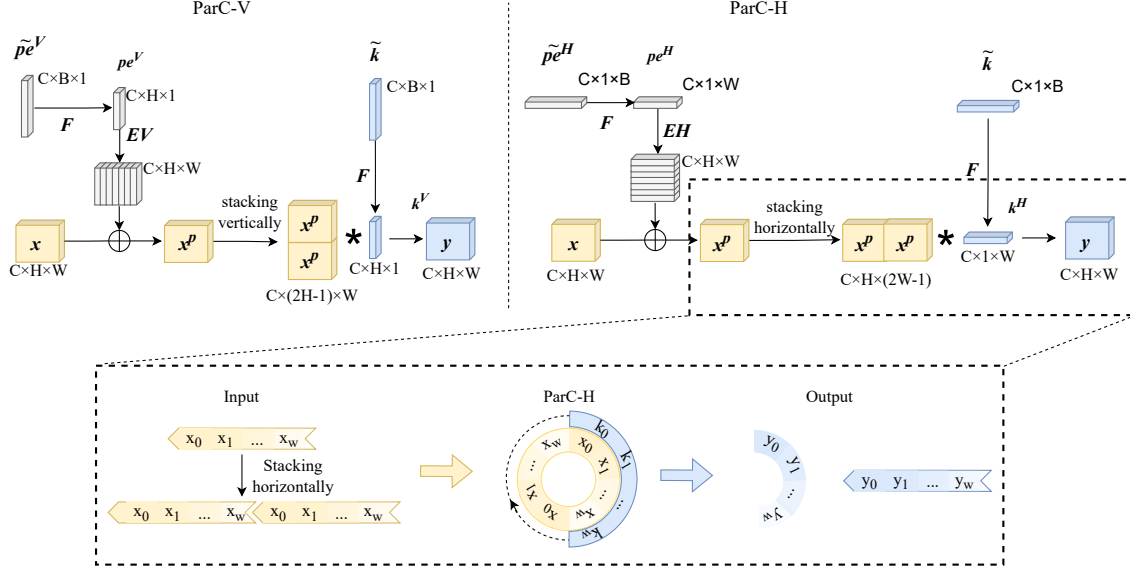


Fig. 2: Illustration of the position aware circular convolution, corresponding with Eq. 2. The circular convolution part is amplified with dash line connection. ParC-H and ParC-V follows similar strategy, but are conducted in different axis.

as $\mathbf{w} = \{w_0, w_1, \dots, w_{K_h-1}\}$. The Pytorch-style convolution (i.e. `F.conv1d`) with zero-padding can then be expressed as:

$$y_i = \sum_{k=0}^{K_h-1} w_k \cdot x_{k+i-K_h/2}, \quad i = 0, 1, \dots, H_y - 1 \quad (1)$$

where $K_h/2$ is used to offset the extra paddings of $K_h/2$ scalars on both sides of the input. Eq. 1 shows that y_i is a function of its local neighboring input (i.e. $x_{i-K_h/2}, \dots, x_{K_h/2-1+i}$), and the size of the neighborhood is controlled by the kernel size K_h . As a consequence, it is impossible for a single layer of small kernel convolution to collect long distance information. To solve this shortcoming of vanilla convolution, we propose our ParC with global receptive field.

3.1.2 ParC: Positional-Aware Circular Convolution

Define $\mathbf{w} = \{w_0, w_1, \dots, w_{K_h-1}\}$ as the kernel weight, and $\mathbf{pe} = \{pe_0, pe_1, \dots, pe_{K_h-1}\}$ as the positional embedding. Corresponding with Fig. 2, ParC could be described as:

$$\begin{aligned} y_i &= \sum_{k=0}^{H-1} w_k^H \cdot (x_{(k+i) \bmod H}^p) \\ \mathbf{w}^H &= f(\mathbf{w}, H) \\ \mathbf{x}^p &= \mathbf{x} + f(\mathbf{pe}, H) \end{aligned} \quad (2)$$

where $i = 0, 1, \dots, H - 1$. w is the learnable kernel of a fixed size (specified by hyper-parameters) and w^H is the adjusted learnable kernel whose size match the corresponding input feature map size. pe denotes position embedding. Here, we adopt interpolation function $f(\cdot, N)$ (e.g. bi-linear, bi-cubic) to adapt the sizes of kernels and position embedding (from K_h to H). \bmod denotes the modulo operation.

Compared to vanilla convolution, the ParC operator has four major differences: 1) global kernel; 2) circular convolution; 3) positional embedding; 4) 1D decomposition. To extract global feature effectively, these designs are all essential, which is demonstrated later by ablation experiments in

Section 4.4. In the following, we will elaborate more on the reasons of these design differences:

Global kernel and Circular Convolution. To extract global relationships across the whole input map, ParC adopts global kernels, the size of which are the same as the size of the corresponding feature maps, denoting as $K_h = H$ or $K_w = W$. In some architectures this is shrunk by half in each stage. For example in ResNet50 or ConvNeXt, the feature resolution are [56, 28, 14, 7] respectively for four stage. But simply enlarging the size of the ordinary convolution kernel itself cannot extract the global relationship effectively. Because of the use of zero padding, even if the kernel size increases to the resolution, the kernel weight will be aligned to the zero paddings, which cannot offer useful information except for absolute location. This effect happens most extremely when kernel is aligned to the edge of a picture - for a 2D convolution, 3/4 of the inputs are actually zeros instead. Therefore, we additionally propose to use the circular convolution. When doing circular convolution, kernel weight are always aligned to valid pixels during window sliding, as is shown in Fig. 2.

Positional Embedding. As concluded in previous work [48], vanilla convolution could encode positional information whenever it uses zero-padding. Circular convolution, however, reuses the input picture in a periodic way, this will lose part of the location information. To conquer this, we introduce learnable position encoding, which is inserted before the circular convolution. In the following experiment, we demonstrate that this is very important for models' performance, especially for downstream tasks which are sensitive to spatial information.

1D Decomposition. Finally, in order to ensure acceptable cost in model size and computation. We split the 2D convolution and position encoding into H (horizontal) and V (vertical) directions, which reduce the number of parameters and FLOPs from $\mathcal{O}(H \times W)$ to $\mathcal{O}(H + W)$, this is a considerable compression when the resolution is large.

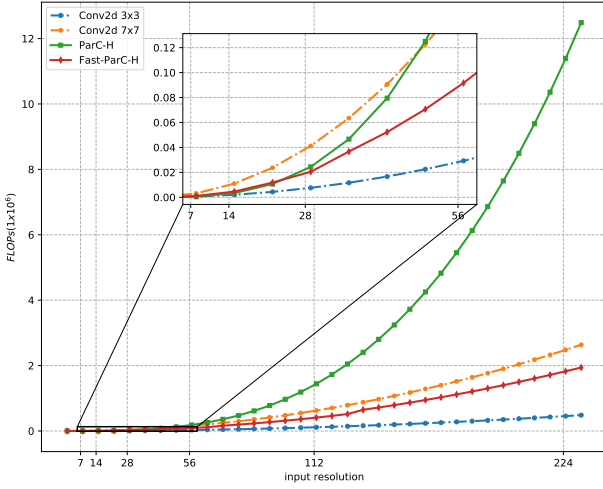


Fig. 3: The theoretical FLOPs of different convolutions operations, estimated with channel number and batch size as 1. Dash line indicates operation is with local receptive field, solid line indicates operation is with global receptive field.

Implementation of Circular Convolution. Conceptually, the circular convolution needs to be implemented separately from ordinary convolutions because of the extra modulus operation when computing the index of convoluted pixels. In practice, it could be easily implemented by padding the input feature map with its copy using ‘concat’ function before calling the ordinary 1D convolution routines (See Algorithm 1)

When considering vertical dimension W and the channel dimension C , the Eq. 2 could be extended as

$$\mathbf{Y}_{i,j,c} = \sum_{k=0}^{H-1} \mathbf{W}_{k,c}^H \cdot (\mathbf{X}_{(k+i) \bmod H,j,c}^p) \quad (3)$$

$\forall i \in [0, H-1], \forall j \in [0, W-1]$ and $\forall c \in [0, C-1]$, which is the full representation of a one layer depth-wise ParC-H with channels C , and input resolution $H \times W$. In ResNet50-ParC, we also extend the per channel ParC to its dense counterpart and reintroduce the channel interaction, which can be expressed as:

$$\mathbf{Y}_{i,j,c_o} = \sum_{c_i=0}^{C_i-1} \sum_{k=0}^{H-1} \mathbf{W}_{k,c_i}^H \cdot (\mathbf{X}_{(k+i) \bmod H,j,c_i}^p) \quad (4)$$

considering $\forall i \in [0, H-1], \forall j \in [0, W-1], \forall c_i \in [0, C_i-1]$ and $\forall c_o \in [0, C_o-1]$.

3.2 Fast-ParC: Speed up ParC with its FFT Equivalent Form

As shown in Fig 3, when feature resolution is small (e.g. 7x7), applying ParC can extract global feature and reduce the computation complexity effectively. But as input resolution grows, the complexity of ParC surpasses 7x7 convolution rapidly. To overcome this issue, we propose an accelerated version of ParC named Fast-ParC. Fast-ParC is much more efficient than ParC when feature resolution is large (e.g. 56x56). In fact, Fast-ParC, while enjoying global extracting ability, is even more efficient than 7x7 convolution within a wide interval of resolution.

Algorithm 1 PyTorch style Pseudo code of ParC-H and Fast-ParC-H. Codes are based on depth-separable version. (H means horizontal. It could be easily extended to ParC-V by conducting these operations in vertical dimension.)

```
# B: batch size, C: channel number
# H: height, W: weight
# fft1d: FFT conduct in one dimension indicates by 'dim'.
# ifft1d: inverse FFT, normalized with 1/N by in default
def ParC_H(x, weight, bias):
    B, C, H, W = x.shape
    # periodic extension
    x_cat = torch.cat([x, x[:, :, :-1, :]], dim=-2)
    # spatial-ParC
    x = F.conv2d(x_cat, weight, bias, padding=0, groups=C)
    return x

def Fast_ParC_H(x, weight, bias):
    B, C, H, W = x.shape
    # input FFT
    x = fft1d(x, dim=-2)
    # weight FFT
    weight = fft1d(weight, dim=-2)
    # Fourier-ParC
    x = x * torch.conj(weight).view(1, C, H, 1)
    # output iFFT
    x = ifft1d(x, dim=-2).real
    x = x + bias.view(1, C, 1, 1)
    return x
```

We derive Fast-ParC with the help of Fast Fourier Transform(FFT). It is well known that linear convolution operation could be facilitated by FFT [50]. But according to convolution theorem [50], for discrete signal, dot product in the Fourier domain is closer to *circular convolution* in spatial domain. This is exactly one of the distinctive differences between ParC and ordinary convolution. In addition, the other two features of ParC, *global kernel* and *right padding*, also fit well with the default mode of convolution in Fourier domain. This interesting fact allows us to develop a very neat and beautiful frequency domain implementation for ParC. Define $x(n)$, $w(n)$, $y(n)$ as input, weight and output sequence in time domain, $X(k)$, $W(k)$ and $Y(k)$ as the sequence in Fourier domain, we could get the following equivalence relationship:

Theorem 1: ParC equivalence theorem

$$\begin{aligned} \text{Spatial Form: } y(n) &= \sum_{i=0}^{N-1} w(i)x((n+i))_N \\ &\Updownarrow \\ \text{Fourier Form: } Y(k) &= W^*(n)X(n) \end{aligned} \quad (5)$$

Eq. 5 shows two mathematical expressions which are strictly equivalent. ParC in spatial domain requires a convolution style operation, however in Fourier domain it turns into a simple per-element multiplication. Based on this, we propose a Fourier domain version of ParC operation, named Fast-ParC. It can be proved theoretically that Fast-ParC is strictly equivalent to ParC in spatial domain (See Appendix A.1). The error between these two implementations is negligible. we can choose the appropriate implementation of

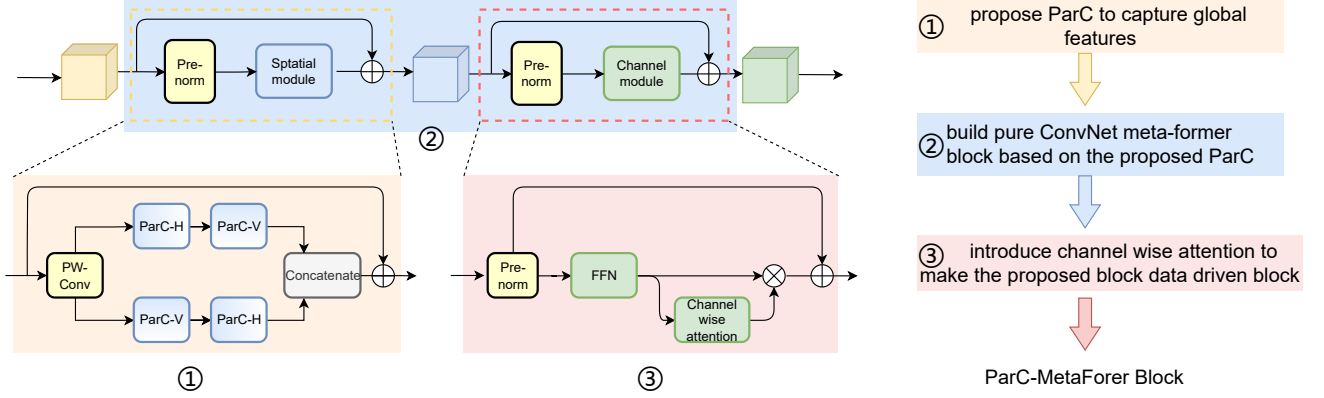


Fig. 4: ParC-MetaFormer block used to replace transformer blocks in ViTs or hybrid structures (e.g. MobileViT [11]). ParC-MetaFormer block adopt a MetaFormer [49] like block structure, and it keeps the 3 merits of transformer block: 1) global receptive field; 2) positional-aware; 3) data-driven.

ParC respectively for training and inference, depending on the platform that are actually used. This provides ParC with powerful flexibility. Algorithm 1 shows the pseudo-code. The advantages of Fast-ParC are clear:

Firstly, the multiplication complexity of 1D-FFT with length N is only $\mathcal{O}(N \log N)$, while 1D convolution in spatial domain requires $\mathcal{O}(N^2)$.

Corresponding with Table 1, it's clear that the complexity of spatial convolution surpasses the FFT-based convolution by a large margin, when N is large. ParC use a global kernel and circular convolution, which matches the default spatial format of Fourier convolution. Considering downstream task like detection or segmentation with multiple instances, usually much higher resolution is needed. For example for COCO [51], the commonly used resolution for testing is 1280×800 , and for ADE20k [52] is 2048×512 . When N is large, Fast-ParC can save model's FLOPs and achieve a better acceleration. Fast-ParC also allows us to use ParC for the shallower stages with a acceptable budget in computation. This is necessary for implementation of ParC in novel architectures [53].

Another advantage actually comes from the software/hardware support for FFT. Since FFT is a classical signal processing algorithm, many platforms have off-the-peg support for its acceleration. When ParC is applied to customized platform like FPGA, many resources (e.g. on-chip DSP, pre-designed IP core) could be utilized effectively. Besides, universal computing platforms have out-of-the-box toolkit for it as well (e.g. CPU: torch.fft [54], numpy.fft [55]; GPU: cuFFT [56]). The flexibility of Fast-ParC allows us to choose the better implementation with respect to different standard (e.g. most throughput, least memory occupation), and with respect to the actual preferences for algorithms in different computing platforms.

Luckily, Fast-ParC is completely equivalent to ParC, and the replacement does not require any additional transformations. We can choose the specific implementation form of ParC according to the requirements of the platform. As ParC and Fast-ParC owns the highest level of flexibility, the implementation used for training and inference could also be decoupled. Further exploration of other efficient convolution operations based on FFT is also a very promising

Operation	Theoretical complexity
Self-Attention	$\mathcal{O}(CH^2W^2 + C^2HW)$
Conv2d	$\mathcal{O}(CHWK_xK_y)$
ParC	$\mathcal{O}(CHW(H+W))$
FFT-ParC	$\mathcal{O}(CHW(\lceil \log_2 H \rceil + \lceil \log_2 W \rceil))$

TABLE 1: The theoretical complexity of multiplication for different convolution operation. The Complexity of FFT-ParC are with base-2-FFT. One complex multiplications are treated as 4 real multiplications.

direction, and we leave this issue for future.

3.3 Applying ParC on ViTs and ConvNets

To validate the effectiveness of ParC as a plug-and-play meta-operator, we built a series of ParC-based Models based on the operations proposed in Section 3.1. Here, baseline models includes both ViTs and ConvNets. Specifically, for ViTs, MobileViT [11] is selected as baseline, as it achieved the best parameter/accuracy trade-off among the lightweight hybrid-structures proposed recently. ResNet50 [28], MobileNetv2 [14] and ConvNext [27] are adopted as ConvNet baselines. ResNet50 is the most widely used model in practical applications. MobileNetV2 is the most popular model in mobile devices. ConvNext is the first ConvNet which remains pure ConvNet architecture while integrates some characteristics of ViTs. All of the four models we adopted here are representative.

3.3.1 ParC-ViTs

ParC-MetaFormer Block. As shown in Fig 4 and Fig 5, ConvNets and ViTs have big difference in outer layer structure. ViTs generally adopt meta-former block as basic architecture. To apply ParC operator on ViTs, we design ParC-MetaFormer block and use it to replace transformer blocks in ViTs.

Adopting MetaFormer like structure. A MetaFormer [49] block is the block structure that ViTs use most frequently, and it generally consists of a sequence of two

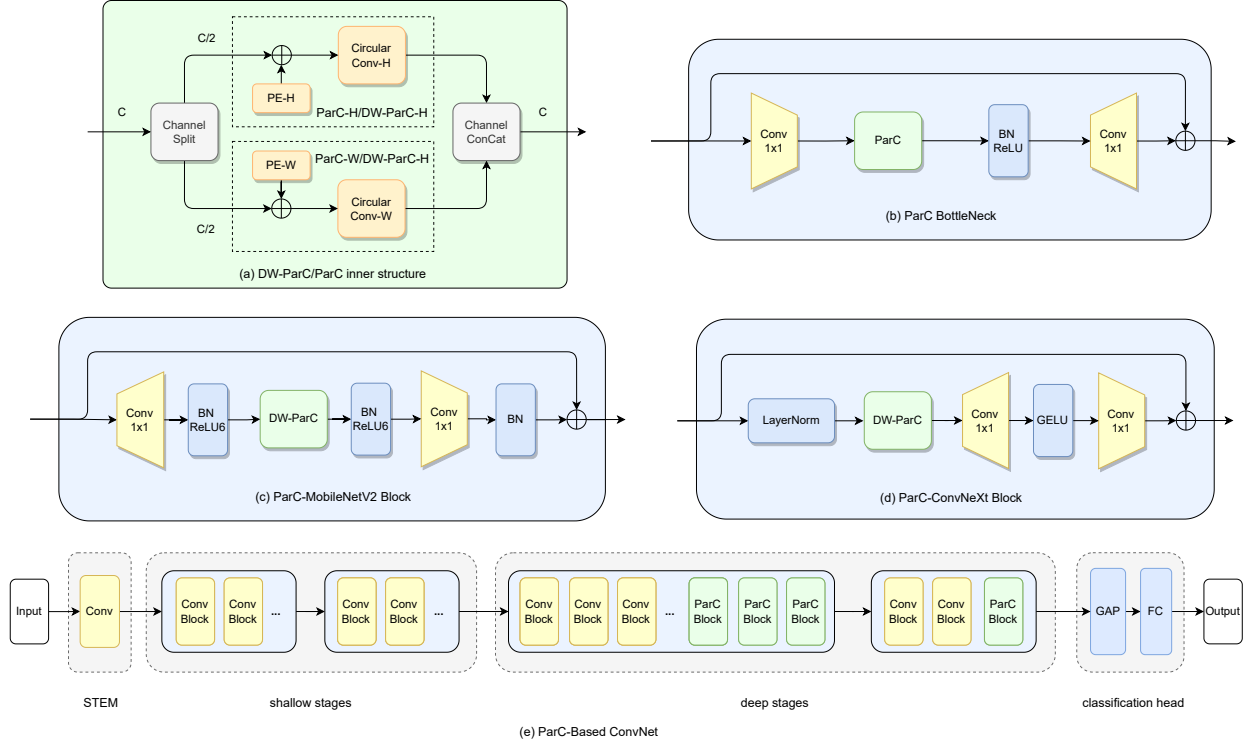


Fig. 5: The hierarchical structure of ParC-based ConvNets. Fig. (a) shows the inner structure of an ParC or Dw-ParC (i.e. depth-wise version ParC) operator. Fig. (b)(c)(d) illustrate 3 different ParC-ConvNet blocks. Fig (e) shows the ParC-ConvNet structure, which indicates we replace the last several blocks in the deep stages and remain the structure in the shallow stages.

components: a token mixer and a channel mixer. Both two components use residual structure. We adopt ParC as a token mixer to build a ParC-MetaFormer block. We do this because ParC can extract global features and interacts information among pixels from global space, which meets the requirement of token mixer module. And unlike the self-attention whose complexity is quadratic, ParC are much more efficient in computation. Replacing this part with ParC can reduce computational cost significantly. In ParC-MetaFormer Block, we adopt a serial structure of ParC-H and ParC-V. Considering symmetry, half of the channels go through ParC-H firstly, and others go through ParC-V firstly (as shown in Fig 4).

Adding channel wise attention in channel mixer part. Though ParC keeps the global receptive field and positional embedding, another benefit ViTs have against ConvNets is data-driven. In ViTs, self attention module can adapt weights according to input. This makes ViTs data-driven models, which can focus on important features and suppress unnecessary ones, bringing better performance. Previous literature [57] [58] [59] already explained the importance of keep model data driven. By replacing the self-attention with the proposed global circular convolution, we get a pure ConvNet which can extract global features. But the replaced model is no longer data-driven. To compensate, we insert channel wise attention module into channel mixer part, as shown in Fig. 4. Following SENet [57], we first aggregate spatial information of input features $x \in \mathbb{R}^{c \times h \times w}$ via global average pooling and get aggregated feature $x_a \in \mathbb{R}^{c \times 1 \times 1}$

Then we feed x_a into a multi-layer perception to generate channel wise weight $a \in \mathbb{R}^{c \times 1 \times 1}$. The a is multiplied with x channel wise to generate the final output.

MobileViT-ParC Network. Currently, existing hybrid structures can be basically divided into three main structures, including serial structure [25] [42], parallel structure [12] and bifurcate structure [11] [24]. Among all three structures, the third one achieves best performance for now. MobileViT [11] also adopts the bifurcate structure. Inspired by this, based on MobileViT, we build our model with bifurcate structure as well. MobileViT consists of two major types of modules. Shallow stages consist of MobileNetV2 blocks, which have local receptive field. Deep stages are made up of ViT blocks, which enjoy global receptive field. We keep all MobileNetV2 blocks and replace all ViT blocks with corresponding ParC blocks. This replacement converts the model from hybrid structure to pure ConvNet, while reserving its global feature extracting ability.

3.3.2 ParC-ConvNets

For ParC-ConvNets, we focus on providing ConvNets with global receptive field. Replacing vanilla convolution with ParC operation (as shown in Fig. 5 (a)), we build different ParC-based blocks (as shown in Fig. 5 (b)(c)(d)). Previous hybrid structure works [25] [42] [11] draw a similar conclusion: models with local-extracting blocks in early stages and global-extracting blocks in deep stages achieve the best performance. Since ParC owns a global receptive field, we insert ParC-based block into ConvNets following this rule (as shown in Fig. 5 (e)).

Frameworks	Models	Source	Params (M)	Top1 Accu (%)
Pre-ConvNet	SuffNetV2(2.0x)	ECCV 2018	5.5	74.5
	MobileNetV3(1.0x)	ICCV 2019	5.4	75.2
	EfficientNet-B0	ICML 2019	5.3	76.3
	ResNet-101-SE	CVPR 2018	49.3	77.6
ViTs	DeiT-2G	ICML 2021	9.5	77.6
	Swin-1G	ICCV 2021	7.3	77.3
Hybrid Structures (ConvNet+ViT)	CoaT-Lite-T	ICCV 2021	5.7	76.6
	LeViT-128S	ICCV 2021	7.8	76.6
	Mobile-Former	CVPR 2022	9.4	76.7
	MobileViT-S [†]	ICLR 2022	5.6	78.4
	EfficientFormer-L1 [†]	arXiv 2022	12.3	76.0
Post-ConvNet	ConvNeXt-XT	CVPR 2022	7.4	77.5
	MobileViT-ParC-S [†]	ECCV 2022	5.0	78.6

TABLE 2: Classification results on ImageNet-1K. [†] means running in MobileViT [11] training framework. Pre-ConvNet indicates classical ConvNets before ViTs appeared, Post-ConvNet integrates merits of both ViTs and ConvNets.

ParC BottleNeck and ResNet50-ParC Network. ResNet [28] is one of the most classical ConvNet. Simply replacing the 3×3 convolution of the original ResNet50 BottleNeck with a ParC operator, we can obtain the ParC BottleNeck (see Fig 5 (b)). Since the characteristics of ParC-H and ParC-V might be significantly different, no channel interaction is introduced between them. This is similar to adopt group convolution [60] with group=2. The main part of ResNet can be divided into 4 stages, and each stage consists of a couple of repeated BottleNeck blocks. Specifically, ResNet50 has [3, 4, 6, 3] blocks respectively in four stages. By replacing the last 1/2 of the penultimate stage of ResNet50 and the last 1/3 of the last stage with ParC BottleNeck, we obtain ResNet50-ParC.

ParC-MobileNetV2 Block and MobileNetV2-ParC Network. MobileNetV2 [14] is a typical representative of the lightweight model. By replacing the 3×3 depthwise convolution in Inverted Bottleneck with depthwise ParC, we get the ParC-MobileNetV2 block (see Fig 5 (c)). MobileNetV2 is much slimmer and deeper than the Resnet50, with blocks number of [1, 2, 3, 4, 3, 3, 1] respectively for 7 stages. MobileNetV2-ParC could be obtained by replacing the last 1/2 blocks of stage 4 and the last 1/3 blocks of stage [5, 6] with ParC-MobileNetV2 blocks.

ParC-ConvNeXt Block and ConvNeXt-ParC Network. ConvNeXt [27] take a sequence of modifications on original ResNet50 structure to learn from transformers. During this, 3×3 convolution is replaced with 7×7 depthwise convolution. This enlarges the local receptive field, however it still cannot grad global information. We further replace 7×7 depthwise convolution in ConvNeXt Block by depthwise ParC. By this we obtain the ParC-ConvNeXt block (see Fig 5 (d)). Replacing the last 1/3 blocks of the last two stages of ConvNeXt with ParC-ConvNeXt blocks, an example of ConvNeXt-ParC is obtained. We reduce the basic channel number in ConvNeXt-T to 48 (i.e. [48, 96, 192, 384] for each stage) to get a light weight ConvNeXt-XT, which is more welcome in deploying on edge computing devices and it also has shorter experimental period.

Note that, in ParC-MetaFormer, a sequence of ParC-H and ParC-W is adopted keep the receptive field consistent with self-attention, as this design is used to replace self-attention. In ParC-ConvNets, we adopt a parallel of ParC-

H and ParC-V (each one single layer) as shown in Fig. 5. According to experimental results, this setting could already provide enough performance gain against the vanilla ConvNets. In fact, as we do not use only one ParC-ConvNet block, the ParC-ConvNets still has global receptive field.

4 EXPERIMENT

To test the capability of ParC as a plug-and-play operator. We applied it to a wide range of models including Transformers and ConvNets. We take different views when plugging ParC into these two kind of models. For transformer models, the main purpose of applying ParC is to make model more hardware friendly while keep its ability of global extracting, thus we use ParC to replace self-attention. For ConvNets, we use ParC mainly to enable networks with global extracting ability, while keeping it parameter/FLOPs friendly, thus we use ParC to replace vanilla convolution.

4.1 Experiment on Vision Transformer Models

In the transformer experiments, we focus on inserting the ParC operator into the most recently proposed MobileViT framework. We show the overall advantages of the proposed MobileViT-ParC on three typical vision tasks, including image classification, object detection and semantic segmentation.

4.1.1 Image Classification on ImageNet-1K

We conduct image classification experiments on ImageNet-1k, the most widely used benchmark dataset for this task. We train the proposed MobileViT-ParC models on the training set of ImageNet-1K, and report top-1 accuracy on the validation set.

Training setting. As we adopt MobileViT like structure as our outer framework, we train our model using a very similar training strategy as well. To be specific, we train each model for 300 epochs on 8 V100 or A100 GPUs with AdamW optimizer [61], where the maximum learning rate, minimum learning rate, weight decay and batchsize are set to 0.004, 0.0004, 0.025 and 1024 respectively. Optimizer momentum β_1 and β_2 of the AdamW optimizer are set to 0.9 and 0.999 respectively. We use the first 3000 iterations as warm up stage. We adjust learning rate following the cosine schedule.

Models	Params (M)	mAP
MobileNetV2	4.3	22.1
MixNet	4.5	22.3
MNASNet	4.9	23.0
MobileViT	2.7	24.8
VGG	35.6	25.1
ResNet50	22.9	25.2
MobileViT-S	5.7	27.7
MobileViT-ParC-S	5.2(↓0.5)	28.8(↑1.1)

Models	Params (M)	mIoU
MobileNetV1	11.2	75.3
MobileNetV2	4.5	75.7
MobileViT-XXS	1.9	73.6
MobileViT-XS	2.9	77.1
ResNet101	22.9	80.5
MobileViT-S	6.4	79.1
MobileViT-ParC-S	5.8(↓0.6)	79.7(↑0.6)

TABLE 3: Object detection results on MS-COCO (Left) and Semantic segmentation experiments on PASCAL VOC (Right) about ParC-based transformer models. We compare the mAP/mIoU with more other models.

For data augmentation, we use random cropping, horizontal flipping and multi-scale sampler. We use label smoothing [62] to regularize the networks and set smoothing factor to 0.1. We use Exponential Moving Average (EMA) [63]. More details of the training settings and link to source code will be provided in supplementary materials.

Results comparison. The experiment results of image classification and comparison with other models are listed in Table 2. Table 2 shows that MobileViT-ParC-S and MobileViT-S beat other model by a clear margin. The proposed MobileViT-ParC-S achieves highest classification accuracy, and have fewer parameters than most models. Compared with the second best model MobileViT-S, our MobileViT-ParC-S decreases the number of parameters by 11% and increases the top-1 accuracy by 0.2 percentage. Light-weight models. Firstly, comparing results of light-weight ConvNets with that of ViTs, light-weight ConvNets show much better performance. Secondly, comparing the popular ConvNets before ViT appears (pre-ConvNets), ViTs and hybrid structures, hybrid structures achieve the best performance. Therefore improving ConvNets by learning from the merits of ViT is feasible. Finally, the proposed MobileViT-ParC achieves the best performance among all comparison models. So indeed by learning from ViT design, performance of pure light-weight ConvNets can be improved significantly.

4.1.2 Object detection on MS-COCO

We use MS-COCO [64] datasets and its evaluation protocol for object detection experiments. Following [14] [11], we take single shot object detection (SSD) [65] as the detection framework and use separable convolution to replace the standard convolutions in the detection head.

Experiment setting. Taking models pretrained on ImageNet-1K as backbone, we finetune detection models on training set of MS-COCO with AdamW optimizer for 200 epochs. Batchsize and weight decay are set to 128 and 0.01. We use the first 500 iterations as warm up stage, where the learning rate is increased from 0.000001 to 0.0009. Both label smoothing and EMA are used during training.

Results comparison. Table 3 lists the corresponding results. Similar to results in image classification, MobileViT-S and MobileViT-ParC-S achieve the the second best and the best in terms of mAP. Compared with the baseline model, MobileViT-ParC-S shows advantages in both model size and detection accuracy.

Row	Model	Params (M)	FLOPs (G)	Top1 Accu (%)
1	ResNet50	25.6	4.1	79.1
2	ResNet50-ParC	23.7	4.0	79.6(↑0.5)
3	MobileNetV2	3.51	0.6	70.2
4	MobileNetV2-ParC	3.54	0.6	71.1(↑0.9)
5	ConvNeXt-Xt	7.44	1.1	77.5
6	ConvNeXt-ParC-Xt	7.41	1.1	78.3(↑0.8)

TABLE 4: Classification results on ImageNet-1K about ParC based ConvNets. All models are running in ConvNext’s [27] training recipe.

4.1.3 Semantic segmentation on VOC/COCO

Experiment setting. DeepLabV3 is adopted as the semantic segmentation framework. We fine tune segmentation models on training set of PASCAL VOC [66] and COCO [51] dataset, then evaluate trained models on validation set of PASCAL VOC using mean intersection over union (mIoU) and report the final results for comparison. We fine tune each model for 50 epochs with AdamW. Readers may refer to more details about training settings in supplementary materials.

Results comparison. Results are summarized in Table 3. We can see that MobileViT-S and MobileViT-ParC-S have the best trade-off between model scale and mIoU. Compared with ResNet-101, MobileViT-S and MobileViT-ParC-S achieve competitive mIoU, while having much fewer parameters.

4.2 Experiment on Convolutional Models

In the convolutional networks experiment, we insert the ParC module into ResNet50, MobileNetV2 and ConvNeXt. These part of experiments also include the three typical vision tasks, classification, detection and segmentation. All of the following models are trained and evaluated under ConvNeXt’s [27] settings.

4.2.1 Image Classification on ImageNet-1K

Training setting. Most of our training settings for convolutional models are from ConvNeXt’s [27] guide. To be specific, we use 8 2080Ti or 3090 to train each model for 300 epochs, with AdamW optimizer. The learning rate increase linearly in the beginning 20 epochs as warm-up, and then decay with cosine schedule. The batch size, base learning rate, weight decay, momentum β_1 and β_2 are setting as 4096, 0.004, 0.05, 0.9 and 0.999, respectively. Data augmentations used include Mixup, Cutmix, RandAugment, and Random

Backbone		Instance Detection						Instance Segmentation					
Model	Params (M)	AP ^{box}	AP ₅₀ ^{box}	AP ₇₅ ^{box}	AP _S ^{box}	AP _M ^{box}	AP _L ^{box}	AP ^{mask}	AP ₅₀ ^{mask}	AP ₇₅ ^{mask}	AP _S ^{mask}	AP _M ^{mask}	AP _L ^{mask}
ResNet50	25.6	47.5	65.6	51.6	29.9	51.1	61.5	41.1	63.1	44.6	23.6	44.7	55.3
Resnet50-ParC	23.7(↓1.9)	48.1(↑0.6)	66.4	52.3	30.3	51.2	62.3	41.8(↑0.7)	64.0	45.1	24.6	45.2	56.0
MobileNetV2	3.51	43.7	61.9	47.6	27.0	46.1	58.3	37.9	59.1	40.8	21.4	40.5	52.5
MobileNetV2-ParC [†]	3.54	44.3(↑0.6)	62.7	47.8	28.0	47.0	58.6	39.0(↑1.1)	60.3	42.1	23.0	41.8	53.1
ConvNeXt-XT	7.44	47.2	65.6	51.4	30.1	50.2	62.3	41.0	62.9	44.2	23.8	44.2	55.9
ConvNext-ParC-XT	7.41	47.7(↑0.5)	66.2	52.0	30.4	50.9	62.7	41.5(↑0.5)	63.6	44.6	24.4	44.7	56.5

TABLE 5: Instance detection and segmentation results on COCO dataset of convolution models and ParC-based convolution models. Code is based on MMDetection. [†] means a 3x expansion of learnable parameters to ParC weight is applied when transferred from ImageNet (i.e. size 224x224) to COCO (i.e. size 800x1333).

Backbone		Evaluation w/o TTA			Evaluation w/ TTA		
Model	Params (M)	mIoU	mAcc	aAcc	mIoU _{aug}	mAcc _{aug}	aAcc _{aug}
ResNet50	25.6	42.27	52.91	79.88	43.75	53.50	80.71
ResNet50-ParC	23.7(↓1.9)	44.32(↑2.05)	54.66	80.80	44.69(↑0.94)	54.38	81.33
MobileNetV2	3.51	38.66	48.75	77.98	39.26	48.27	78.87
MobileNetV2-ParC [†]	3.54	39.25(↑0.59)	49.64	78.35	39.62(↑0.36)	48.57	79.03
ConvNeXt-XT	7.44	42.17	54.18	79.72	43.07	54.27	80.44
ConvNeXt-ParC-XT	7.41	42.32(↑1.15)	54.48	80.30	43.09(↑0.02)	54.41	80.76

TABLE 6: Sementic segmenation result on ADE20k dataset of convolution models and ParC-based convolution models. Test Time Argumentation(TTA) schemes used by us include multi-scaling of [0.5, 1.75] and flipping. [†] means a 4x expansion of learnable parameters to ParC weight is applied when transferred from ImageNet (i.e. size 224x224) to ADE20k (i.e. size 512x2048).

Erasing. Regularization method used include Stochastic Depth [67] and Label Smoothing [62]. Notice in this section **NO** Exponential Moving Average (EMA) skill is used, since in most experiment we observed that the original model owns a higher accuracy than its EMA counterpart.

Results comparison. We show the results of different types ConvNets on ImageNet-1K at Table 4. It's clear that all of the three ParC enhanced models beat their prototypes. Especially for ResNet50, using ParC design improves classification accuracy by 0.5%, while reducing 2M parameters and saving computation cost slightly. Comparing lightweight model MobileNetV2 and MobileNetV2-ParC, our operator shows a extremely obvious advantage with an improvement of 0.9%, with a slightly cost on latency. ConvNeXt-ParC-XT exceed original ConvNeXt-XT by 0.8%, too. Generally speaking, ParC-based convolutional models have almost the same FLOPs and parameters with the original models, but have higher accuracy.

4.2.2 Instance detection and segmentation on COCO

Training setting. We use ConvNets pretrained on ImageNet (in Section 4.2.1) as backbones and then fine-tune with Cascade Mask-RCNN [68] as detection framework on COCO dataset [51]. We set epoch as 36, learning rate as 2e-4 (decays by 10 at epoch 27 and 33). We set momentum β_1 and β_2 as 0.9 and 0.999, weight decay as 0.05, stochastic depth as 0.4. The code is built base on the official implementation of MMDetection [69] toolboxes. FP16 training is NOT used for precision concern. While training ResNet50 and ResNet50-ParC, we frozen the first stage of models. To train ConvNeXt-XT and ConvNeXt-ParC-XT, we set the basic layer-wise learning rate decay to 0.7. For training networks

with Batch Normalization (BN) layers, we set BN layers to evaluation mode throughout the whole process. We use muti-scale training on training set and report the box AP and mask AP on validation set. More detailed training and testing configurations could be seen in our repository.

For MobileNetV2-ParC, since the resolution amplification in our training recipes is about 3 times from ImageNet (224x224) to COCO (800x1333). Specifically, taking ParC kernels in stage 3 as an example, we extend 14x1-sized ParC-H kernels and 1x14-sized ParC-W kernels to 21x1 and 1x42 respectively. We extend kernels pretrained on Imagenet-1K to as initialization kernels for detection and segmentation models.

Results comparison. The result of instance detection and segmentation is listed in Table 5, which is almost consistent with the classification result on ImageNet. The ParC-based models outperform the vanilla models by a clear margin in both box AP and mask AP. Specifically, ResNet50-ParC improves by 0.6 in box AP and 0.7 in mask AP, MobileNetV2-ParC improves by 0.6 in box AP and 1.1 in mask AP, ConvNeXt-ParC-XT improves by 0.5 in both box AP and mask AP.

4.2.3 Semantic segmentation on ADE20K

Training setting. We use convolutional model pretrained on ImageNet as backbone and fine-tune with UperNet [70] as the framework on ADE20K [52] dataset. We set max iteration to 16000. We set basic learning rate as 1, using a linear warmup and the a poly deacy schedule. We set momentum, β_1 and β_2 to 0.9, 0.9 and 0.999, respectively. Weight decay and stochastic depth are set to 0.05 and 0.4. The code is built base on the official implementation of

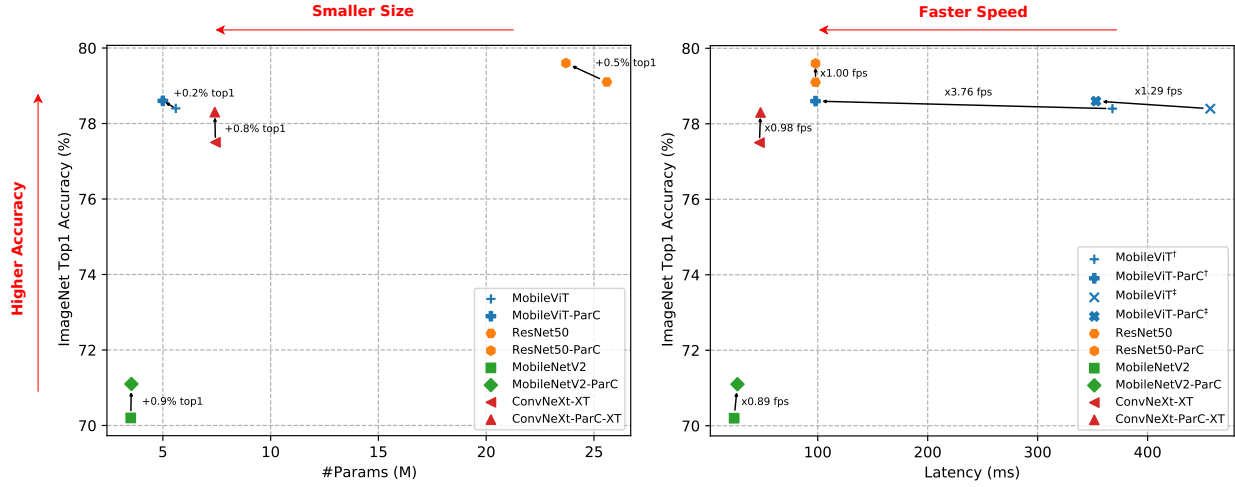


Fig. 6: The parameters-accuracy trade-off (left) and latency-accuracy trade-off (right) of ParC-based models and their vanilla counterparts. Arrows in the left figure indicate the accuracy changes, in the right figure indicate the latency changes. † and ‡ indicate results measured on different platforms (see Table 7 for detail.) Figures show that: 1) Replacing self-attention with ParC decreases ViTs’ parameters/latency drastically, with slight improvement in performance; 2) Replacing convolution with ParC improves the performance over a wide range of ConvNets, with slight growth in models’ parameters/latency.

MMSegmentation [71] toolboxes. F16 training is **NOT** used for precision concern. For networks with BN, setting all BN layer to evaluation mode during fine-tuning. We froze the first stage of ResNet50 and ResNet50-ParC. For ConvNeXt-XT and ConvNeXt-ParC-XT, we use a basic layer-wise learning rate decay of 0.9. For MobileNetV2-ParC, we extend the learnable parameters of ParC to its 4×times and use the interpolation result as initialization. We do this adaptation step because the resolution of ADE20k (i.e. 512×2048) is larger than ImageNet (i.e. 224×224). We use multi-scale training and report mIoU, mAcc and aAcc results on validation set. Follow ConvNeXt [27] and Swin [23], we enable ‘slide’ mode during evaluation. By doing this, the original picture would be cut into several patches and passed to network individually. Specifically, we set crop size as 512×512, stride as 341 (take the average for overlapping area). We test the original single-scale mIoU, and also the mIoU with test time argumentation (TTA). The TTA used include: 1) flipping; 2) multi-scaling of range [0.5, 1.75]. Result are shown in Table 6.

Results comparison. The ParC models improves a lot to be compared with the original models. Inserting ParC operation improves about 1.15 in ConvNeXt-XT. In traditional network, it has a even better performance. Especially, ResNet50-ParC outperforms the original ResNet50 by 2.05, MobileNetV2-ParC outperforms MobileNetV2 by 0.59 in mIoU. TTA improves performance for all ConvNet models test here. But, it is clear that vanilla ConvNets could get more benefit from it. Comparing the row 3-5 with row 6-8 in Table 6, we could conclude that ParC’s advantage degrades significantly after TTA. Even so, ParC version models still show better performance than the vanilla version.

Another interesting fact is that: this significant performance gain is closely related to the ‘512×512-sized crop’ strategy during evaluation. If we set the test mode to ‘whole’, which means to feed the whole 512×2048-sized picture to network, we could also observe a degradation

of ParC-based models’ advantage. This is in accord with what we see when enabling TTA. Based on these results, we conclude one possible explanation - ParC is not robust enough to resolution change. While using ImageNet-1K for pre-training, we empirically set the meta-kernel size to 14 or 7 and use bi-linear interpolation to get a global kernel during practical forward process. Though interpolated kernel works, but it might be a sub-optimum technique, causing instability to resolution changes. A more promising technique is to generate the kernel dynamically. And since zero-padding convolution does not change the resolution of feature map, it might be a candidate for kernel generating module. But we unfortunately failed to accomplish such a version with better performance than Static-ParC, and this might related with normalization or optimization problem. But after all, Dynamic-ParC is still a promising direction for future work.

4.3 Inference Speed Test

In this section, we offer the latency experiments of ParC-based networks measured on multiple platforms. These experiments are conducted to demonstrate two facts:

- 1) ParC could significantly reduce inference latency, when applied to transformer models. To demonstrate this, we deploy MobileViT-ParC on a widely used low power chip Rockchip RK3288, and an in house low power neural network processor DP2000. We use ONNX [72] and MNN [73] to port these models to chips and time each model for 100 iterations to measure the average inference speed. The latency result is then compared with the vanilla MobileViT.
- 2) ParC could significantly boost models’ performance with a negligible increase in complexity, when applied to convolutional models. To demonstrate this, we measure the parameters, FLOPs and latency of ParC-based ConvNets on Xeon E5-2680 v4 CPU. The result is then compared with their vanilla counterparts.

Model	Parms (M)	FLOPs (G)	Devices	Speed (ms)	Top1 Accu (%)
MobileViT-S	5.6	4.0	RK3288	457	78.4
MobileViT-ParC-S	5.0	3.5	RK3288	353	78.6
MobileViT-S	5.6	4.0	DP2000	368	78.4
MobileViT-ParC-S	5.0	3.5	DP2000	98	78.6
ResNet50*	26	4.1	CPU	98	79.1
ResNet50-ParC*	24	4.0	CPU	98	79.6
MobileNetV2*	3.5	0.6	CPU	24	70.2
MobileNetV2-ParC*	3.5	0.6	CPU	27	71.1
ConvNeXt-XT*	7.4	1.1	CPU	47	77.5
ConvNeXt-ParC-XT*	7.4	1.1	CPU	48	78.3

TABLE 7: Applying ParC-Net designs on different backbones and comparing inference speeds of different models. CPU used here is Xeon E5-2680 v4, DP2000 is the code name of a in house unpublished low power neural network processor that highly optimizes the convolutions. * denotes the models are trained under ConvNeXt [27] hyperparameters settings, which may not be the optimal. Latency is measured with batch size 1.

Row	Task	Kernel	CA	PE	Params (M)	Top1/mAP/mIoU
1	Classification	Baseline	-	-	5.6	78.35
2	Classification	BK $L/2$	T	F	5.0	78.46
3	Classification	BK $L/4$	T	F	5.0	78.45
4	Classification	ParC	F	F	5.3	78.50
5	Classification	ParC	T	F	5.0	78.63
6	Classification	ParC	T	T	5.0	78.63
7	Detection	Baseline	-	-	5.7	27.70
8	Detection	ParC	T	F	5.7	27.50
9	Detection	ParC	T	T	5.7	28.50
10	Segmentation	Baseline	-	-	6.4	79.10
11	Segmentation	ParC	T	F	5.8	79.20
12	Segmentation	ParC	T	T	5.8	79.70

TABLE 8: Ablation study conducting conducted under the framework of MobileViT [11]. BK L/n denotes Big kernel with length of $1/n$ times L (resolution), CA denotes channel-wise attention, and PE denotes position embedding.

Model	Params (M)	Global Kernel	Positional Embedding	Circular Convolution	ImageNet Top1 Accu (%)
ConvNeXt-XT	7.44	-	-	-	77.5
ConvNeXt-BK-XT	7.40	T	F	F	77.8
ConvNeXt-ParC-XT	7.41	T	T	T	78.3

TABLE 9: Ablation study conducting conducted under the framework of ConvNeXt [27]. Table shows that applying a big kernel but without circular padding cannot boost the performance maximally.

As shown in row 1-4 of Table 7, compared with baseline, ParC-Net is 23% faster on Rockchip RK3288 and 3.77× faster On DP2000. Besides less FLOPs operations, we believe this speed improvement is also brought by two factors: a) Convolutions are highly optimized by existing tool chains that are widely used to deploy models into these resource constrained devices; b) Compared with convolutions, transformers are more data bandwidth demanding as computing the attention map involves two large matrices K and Q , whereas in convolutions the kernel is a rather small matrix compared with the input feature map. In case the bandwidth requirement exceeds that of the chip design, the CPU will be left idle waiting for data, resulting in lower CPU utilization and overall slower inference speed.

Results in rows 5-10 show that our proposed ParC-Net universally improves performances of common ConvNets. For ResNet50 (rows 5-6), it improves accuracy by 0.5 with less parameters and FLOPs, and almost bring no increase to latency. For MobileNetV2 (rows 7-8) and ConvNeXt (rows

9-10), it improves by 0.9 with slightly increase on budget.

As is illustrated in Fig. 6, by simply replacing the self-attention or convolution operation with our new operator: 1) our ParC op improves accuracy of transformer models by 0.2% on ImageNet classification task and saves as much as 73% of its inference latency; 2) It improves performance of ConvNets by 0.9% at most in accuracy on the same task without introducing obvious negative impacts on inference speed and model size. These results demonstrate that ParC, as a plug-and-play operator, can be plug into different models for different purpose. But whether be apply to ViTs or ConvNets, ParC-based models always have a satisfactory trade-off between performance and complexity.

4.4 Ablation Study

Using the MobileViT as a baseline model, we further conduct ablation analysis to verify the effectiveness of the 2 components we proposed in our ParC-MetaFormer block, Table 8 shows the results.

Framework	Training	Testing	Top1 Accu (%)	Row
ConvNeXt-XT	Vanilla	Vanilla	77.52%	1
	ParC	ParC	78.31%	2
		Fast-ParC	78.31%	3

TABLE 10: ConvNeXt-XT with different implementations of ParC. Result shows that switching between Fast-ParC and ParC could be done without any extra-transition step.

- 1) **Positional Aware Circular Convolution.** The proposed ParC has two major characteristics: a) Circular convolution brings global receptive field; b) PE keeps spatial structure information. Experiment results confirm that both characteristics are important. Results in rows 1-3 show that, using big kernel can also improve accuracy, but the benefit of it reaches a saturation point when kernel size reaches a certain level. This results are consistent with the statement claimed in [27]. Using ParC can further improve accuracy, as shown in rows 2-3 and 5-6. Introducing PE to ParC is also necessary. As we explained in Section 3.1.2, using circular convolution alone can indeed capture global features but it disturbs the original spatial structures. For classification task, PE has no impact (rows 5-6). However, for detection and segmentation tasks which are sensitive to spatial location, abandoning PE hurts performances (rows 9-10 and 12-13).
- 2) **Channel Wise Attention.** Results in rows 4 and 5 show that using channel wise attention can improves performance. But compared with ParC, adopting channel wise attention bring less benefit to model, which indicates that the ParC is the main beneficial component in ParC-MetaFormer block.

Table 9 further shows the ablation analysis we conducted on ConvNeXt's framework. In ConvNeXt-BK-XT, we adopt a vanilla large kernel the same size as stage resolutions (i.e. 13 and 7), but no positional embedding and circular convolution are used. Result shows that the ParC still owns a significant advantage. This is consistent with the shortcomings of vanilla convolution that we mentioned in Section 3.1.2.

In summary, ParC has two key designs: 1) adopting circular convolution with global kernel to ensure the global receptive field; 2) using position embedding to keep position sensitiveness. Both are important.

4.5 Fast-ParC Experiments

In Section 3.2 we proposed Fast-ParC, which could offer as an more efficient alternative for ParC when input resolution is large. It can be theoretically proved that Fast-ParC is equivalent to ParC. In this Section, we further demonstrate these two attributes, equivalence and acceleration, by experiment.

Equivalence Test. To prove the equivalence of ParC and Fast-ParC in real neural networks, we choose ConvNeXt-XT as framework and apply it with ParC or Fast-ParC.

Result listed in Table 10 shows that the switching between Fast-ParC and ParC need no extra transition step. Based on our code implementation, it is easy to verify that

Resolution	Operation	FLOPs (M)	Latency (ms)	Row
28x28	DWConv2d 3x3	0.68	0.07	1
	DWConv2d 7x7	3.69	0.09	2
	ParC	2.11	0.34	3
	Fast-ParC	1.83	0.38	4
56x56	DW-Conv2d 3x3	2.70	0.97	5
	DW-Conv2d 7x7	14.8	1.00	6
	ParC	16.9	1.94	7
	Fast-ParC	8.49	0.79	8
112x112	DW-Conv2d 3x3	10.8	3.16	9
	DW-Conv2d 7x7	59.0	3.10	10
	ParC	134	9.09	11
	Fast-ParC	38.7	5.08	12
224x224	DW-Conv2d 3x3	43.4	12.8	13
	DW-Conv2d 7x7	236	13.2	14
	ParC	1079	44.2	15
	Fast-ParC	174	18.5	16

TABLE 11: The actual inference latency of different operations under different resolution. Tests are conducted with CPU as Intel(R) Core(TM) i7-11800H, torch=1.12.0. We set input batch size as 1, channels number as 96, resolution as 28, 56, 112, 224 respectively.

the magnitude of the error between the outputs of Fast-ParC and ParC is about $1e-7$ averagely. Comparing row 2 with 3, we could draw the conclusion that this error is acceptable for deep neural network, the switching between Fast-ParC and ParC does not affect inference. This result proves the equivalence of ParC and Fast-ParC, and demonstrates that one could choose the better form of ParC according to the actual running experiment.

Latency Test. To test the actual acceleration improvement that Fast-ParC provided, we measure the latency of different operators on Intel(R) Core(TM) i7-11800H for comparison. We test the latency of one single convolution layer. We set the input batch size as 1, channel and dimension as 96, and choose several commonly used resolutions (i.e. 28, 56, 112, 224). Under each resolution setting, we report the latency of Conv2d with kernel size 3x3, Conv2d with kernel size 7x7, ParC and Fast-ParC. Each operation need to repeat for 200 times as warm-up, and then repeat 100 times for actual latency measuring. We use rfft/irfft instead of fft/ifft to further speed up the calculation and save storage.

As shown in Table 11, compared with ParC, Fast-ParC is more efficient in FLOPs and has some advantages in run-time latency. Overall speaking, row 7-8, 11-12, 15-16 still show that Fast-ParC are indeed faster than ParC when input resolution is large. For example with resolution as 224x224, Fast-ParC are 2.39 times faster than ParC. This is corresponding with the theoretical analysis we given in Section 3.2. Row 3-4 show that when resolution is relatively small, like 28x28, the advantage brought by Fast-ParC might be covered by its shortcoming (e.g. paralleling, memory requirement), thus the acceleration effect is not obvious. Therefore, we recommend the use of Fast-ParC when the resolution is large, especially for downstream tasks such as classification and detection. Besides, choosing the proper form according to actual resolution during run-time might also be a feasible strategy. For example, according to Table 11, we could set a threshold of 56, to distinguish whether to use ParC or Fast-ParC during actual run-time.

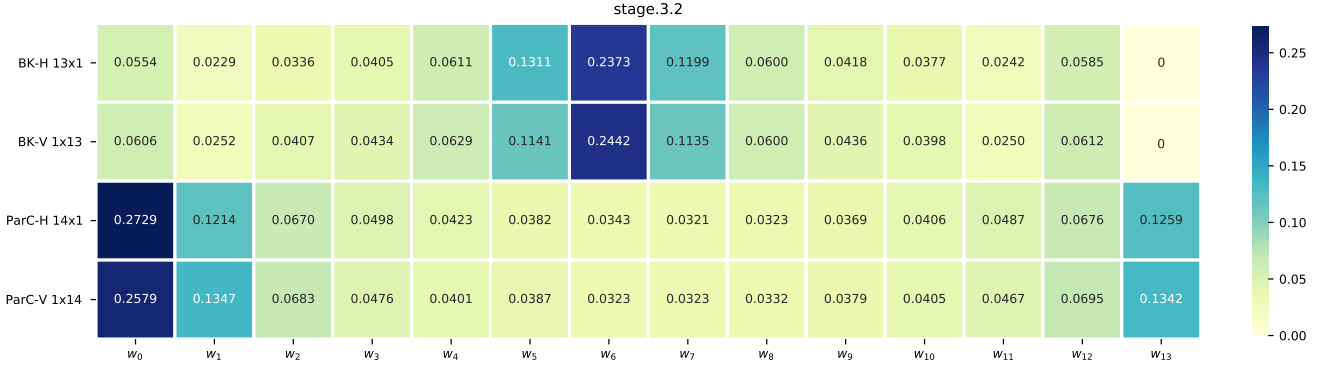


Fig. 7: Spatial weight distributions of 1D Big Kernel (BK) and ParC of the 7th block of stage 3, respectively sampled from ConvNeXt-BK-XT and ConvNeXt-ParC-XT. Weight at each spatial location is calculated with the mean absolute value of all channels with in one layer. Clearly, weights learnt by vanilla big kernel convolution and ParC follow different spatial distributions.

5 DISCUSSION

In this section, we firstly analyze the spatial distribution of weight learnt by of vanilla convolution and ParC. Base on it, we further elaborate that they still learn a similar feature extraction pattern.

Besides, to analyze the mechanism about ParC, we provide the result of two commonly used visualization scheme, Effective Receptive Field (ERF) [15] and Grad-CAM [29]. Result shows that ParC-based models are able to grab global feature even under high resolution, and this makes model more comprehensive when capture instance related semantic information.

5.1 Different Spatial Weights Distribution

We visualize kernels learned in big kernel traditional convolution and our proposed ParC convolution and show them in Fig.7. An interesting phenomenon is found here. In kernels of traditional convolution, from middle to both sides, values range from big to small. Differently, kernels of ParC exactly present an opposite distribution. However, when we take the $K_h/2$ -sized shift into consideration, two kind of distribution will be the same.

In summary, although the proposed ParC summing up information in a different way, it inherently follows the feature extraction rule in traditional convolution.

5.2 ParC Provides Model with Global Effective Receptive Field

Based on Fig 1, we can draw several conclusions:

- 1) **ParC-ConvNets obtain global effective receptive field.** Notice models with ParC have a clearly larger ERF than the vanilla ConvNets. Vanilla ConvNets mostly focus on the center round area (red) of pictures, and its sensitivity drops quickly as radius grows, usually vanishes in the edge/corner region (dark blue). ParC models however owns a global ERF. Though it focus especially on the cruciform regions (red), it still has non-zero value on other parts (yellow or shallow blue). A more obvious merit is that ParC-ConvNeXt's ERF do not decay radially.

- 2) **ERF from different architectures show significantly different shape.** ResNet50 seems to have a *square* outline, the MobileNetV2 and ConvNext-XT however own a much more *round* outline. This might be closely related with the activation function the networks used (ReLU, ReLU6 and GELU). Similar phenomenon [15] are reported to exist between Sigmoid and ReLU, too. Apart from difference in outline, ConvNeXt's ERF also shows a square shadow inside of its round outline. This might be resulted from its non-overlap downsampling layer. In contrast, ResNet and MobileNetV2 have a round shadow in its round outline.
- 3) **The ERF of ConvNeXt is relatively larger than ResNet50 and MobileNetV2.** This is a reasonable conclusion - since ConvNeXt use 7×7 kernel to replace 3×3 kernel in ResNet50. However, this only expands local receptive fields, thus figure shows that in vanilla ConvNeXt-XT's ERF, the magnitude still decays radially. ParC integrate global information, offering ConvNeXt-ParC-XT a effective receptive field over the whole image. As a consequence, ConvNeXt-ParC-XT obtain a better performance, indicating that vanilla large kernels are not as good as global kernels. A parallel work, RepLKNet [16], also mentioned that increasing kernel size of ConvNeXt further to 31×31 could be beneficial.

5.3 ParC Helps Model to form More Comprehensive Focuses

The proposed ParC-based models generally follow this rule: extract local information in its shallow layer, then integrate global information in this deeper layer. This helps model to focus on semantic information that might be hard for vanilla models to catch. We utilize Grad-CAM [29] to visualise the semantic important regions of vanilla ConvNets and ParC-ConvNets. From Fig. 8, the benefit brought by ParC in focusing on semantic important regions could be concluded into two major points:

- 1) **For picture with single object, ParC helps model to capture the whole instance, instead of focusing on some specific parts of it.** The images in columns 1,2

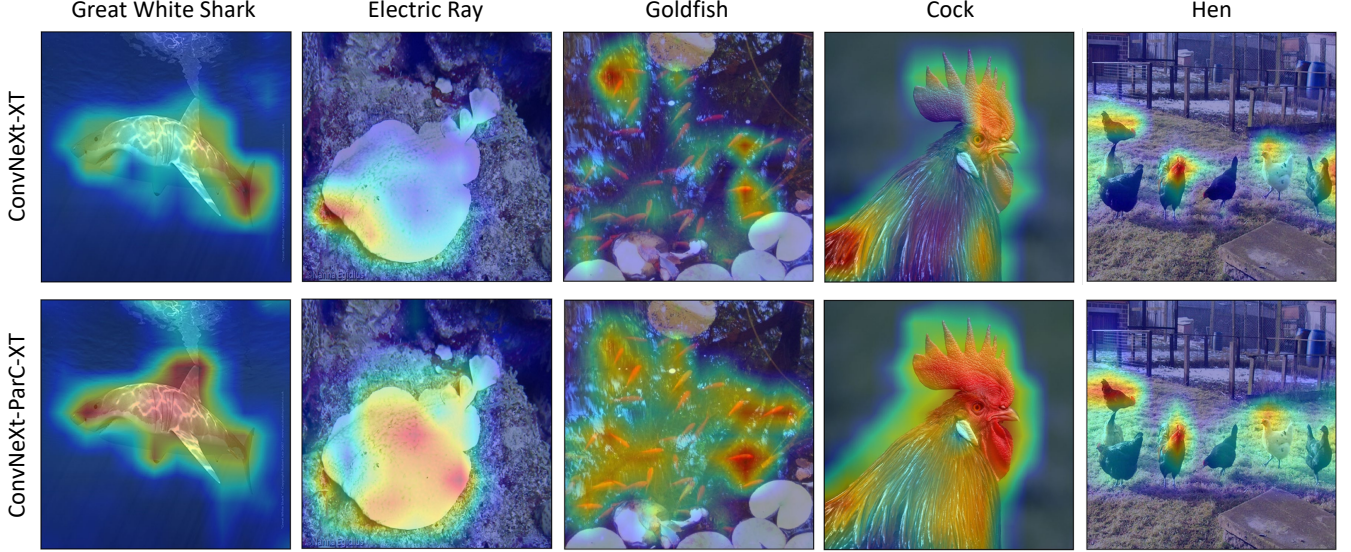


Fig. 8: Grad-CAM visualization of ConvNeXt-ParC-XT and vanilla ConvNeXt-XT.

and 4 could support this state. While capturing features, Vanilla ConvNet focuses on the distinguishing feature like shark tail, cockscomb or the periphery of instances. But ParC-ConvNet seems to have a focus covering the entirely instance, while those distinguishing features are only sub-regions within it.

- 2) **For picture with multiple object, ParC helps model to capture more individuals.** As shown in columns 3 and 5 in Fig 8, when facing a picture with multiple instances, vanilla ConvNet tends to miss some of them but ParC-ConvNet could capture all. This characteristic of ParC might be beneficial for dense prediction task.

6 CONCLUSION

We design a novel plug-and-play operator named ParC (Positional Aware Circular Convolution). ParC owns a global receptive field like self-attention used in ViT, but could be supported more conveniently by different hardware platforms since it use pure convolution operation. We demonstrate it boosts networks' performance on classification whether to be inserted on transformer based networks or convolution based networks. Besides, these ParC-based models shows superiority on downstream tasks as well. We also analyzed the inner mechanism and its difference comparing with vanilla big kernel convolution, and then give some convincing explanations to its superiority. Fast-ParC, an FFT-based version of ParC is also proposed for applying ParC in condition of large resolution. Fast-ParC operation is capable of maintaining low computation budget even with high input resolution, making ParC a competitive general choice for most of computer vision tasks.

APPENDIX A

A.1 Proof of Equivalence of ParC and Fast-ParC

To reuse the classical expression form in signal analysis, a vector of length N could be considered as a discrete

sequence with N non-zero points, namely:

$$\mathbf{x} = \{x_1, x_2, \dots, x_{N-1}\} \iff x(n), \quad 0 \leq n \leq N-1$$

Besides, we use $((x(n)))_N$ to represent the periodic extension with N points for sequence $x(n)$.

We first introduce an property of the sum of periodic sequence before get into Discrete Fourier Transformer (DFT), because it will be frequently used in the proof of following lemmas. For sequence $x((n))_N$, which is with period N . The following lemma always holds:

Lemma 1: Sum of Periodic Sequence

$$\sum_{i=0}^{N-1} ((x(n)))_N = \sum_{i=m}^{N+m-1} ((x(n)))_N, \quad \forall m \in \mathcal{N} \quad (6)$$

This lemma shows the sum of any N successive points of a periodic sequence with period N is the same, which is trivial and thus we give it without a proof.

Usually, the DFT of a N point sequence is still a N point sequence, so we use the following expression to denote a pair of sequences that are counterpart in Fourier domain and spatial domain:

$$\begin{aligned} \mathcal{F}^{-1}\{X(k)\} &= x(n), & 0 \leq n \leq N-1 \\ \mathcal{F}\{x(n)\} &= X(k), & 0 \leq k \leq N-1 \end{aligned}$$

while \mathcal{F} and \mathcal{F}^{-1} indicate the DFT and IDFT respectively. The specific mathematical expression of DFT and IDFT could be denoted as:

$$\begin{aligned} X(k) &= \sum_{n=0}^{N-1} x(n) e^{-j \frac{2\pi}{N} nk} = \sum_{n=0}^{N-1} x(n) W_N^{nk} \\ x(n) &= \sum_{k=0}^{N-1} \frac{1}{N} X(k) e^{j \frac{2\pi}{N} nk} = \sum_{k=0}^{N-1} \frac{1}{N} X(k) W_N^{-nk} \end{aligned}$$

in which $W_N^k = e^{-j \frac{2\pi}{N} k}$ is used as a shorthand.

There exist many exquisite transformation relation for $x(n)$ and $X(k)$, among which the time-domain shifting

property and time-domain flipping property are two commonly used theorems. They which could be written as follows:

Lemma 2: Time-domain Flipping Property

$$\begin{aligned}\mathcal{F}\{x((-n))_N\} &= \sum_{n=0}^{N-1} x((-n))_N W_N^{nk} \\ &= X^*(k)\end{aligned}\quad (7)$$

in which $(\cdot)^*$ indicates the conjugate of \cdot .

Lemma 3: Time-Domain Shifting Property

$$\begin{aligned}\mathcal{F}\{x((n-m))_N\} &= \sum_{n=0}^{N-1} x((n-m))_N W_N^{nk} \\ &= W_N^{mk} \cdot X(k)\end{aligned}\quad (8)$$

The proof can be easily down with method of substitution, after which Eq. 6 could offer great use of resetting the index to $0 \sim N-1$:

Proof 1: Proof of Lemma 2

$$\begin{aligned}\mathcal{F}\{x((-n))_N\} &= \sum_{n=0}^{N-1} x((-n))_N W_N^{nk} \\ &\stackrel{i=-n}{=} \sum_{i=0}^{-N+1} x((i))_N W_N^{-ik} \\ &= \left[\sum_{i=-N+1}^0 x((i))_N W_N^{ik} \right]^* \\ &= \left[\sum_{i=0}^{N-1} x((i))_N W_N^{ik} \right]^* \quad (\text{Eq. 6}) \\ &= X^*(k)\end{aligned}$$

The proof of lemma 3 follows a similar strategy:

Proof 2: Proof of Lemma 3

$$\begin{aligned}\mathcal{F}\{x((n-m))_N\} &= \sum_{n=0}^{N-1} x((n-m))_N W_N^{nk} \\ &\stackrel{i=n-m}{=} \sum_{i=-m}^{N-1-m} x((i))_N W_N^{(i+m)k} \\ &= W_N^{mk} \left[\sum_{i=-m}^{N-1-m} x((i))_N W_N^{ik} \right] \\ &= W_N^{mk} \left[\sum_{i=0}^{N-1} x((i))_N W_N^{ik} \right] \quad (\text{Eq. 6}) \\ &= W_N^{mk} \cdot X(k)\end{aligned}$$

It's easy to tell that the spatial-ParC we gave in Eq. 5 is equivalent to the classical form of *cross-correlation* operation. The following lemma holds:

Lemma 4: The equivalence between ParC and cross-correlation

$$\begin{aligned}w(n) \otimes x((n))_N &= \sum_{n=0}^{N-1} w(n)x((n+m))_N \\ &= \sum_{n=0}^{N-1} x(n)w((n-m))_N\end{aligned}\quad (9)$$

in which \otimes is used to represent ParC operation. (Notice when we talk about ParC, sometime we omit the positional embedding part cause it can be separated from circular convolution easily, while the latter one takes the majority of computation bottleneck.) This could be proved using a similar strategy as shown in Proof 1 and Proof 2:

Proof 3: Proof of Lemma 4

$$\begin{aligned}w(n) \otimes x((n))_N &= \sum_{n=0}^{N-1} w(n)x((n+m))_N \\ &= \sum_{n=0}^{N-1} w((n))_N x((n+m))_N \\ &\stackrel{i=n+m}{=} \sum_{i=m}^{N-1+m} w((i-m))_N x((i))_N \\ &= \sum_{i=m}^{N-1+m} x((i))_N w((i-m))_N \\ &= \sum_{i=0}^{N-1} x((i))_N w((i-m))_N \quad (\text{Eq. 6}) \\ &= \sum_{i=0}^{N-1} x(i)w((i-m))_N \\ &= \sum_{n=0}^{N-1} x(n)w((n-m))_N\end{aligned}$$

Using the 4 aforementioned lemmas, we could prove the two different implementation shown in Eq. 5 is strictly equivalent:

Proof 4: Proof of ParC Equivalence Theorem 5

$$\begin{aligned}
Y(k) &= \mathcal{F}\{y(n)\} \\
&= \mathcal{F}\left\{\sum_{n=0}^{N-1} w(n)x((n+m))_N\right\} \\
&= \mathcal{F}\left\{\sum_{n=0}^{N-1} x(m)w((n-m))_N\right\} \quad (\text{Eq. 9}) \\
&= \sum_{m=0}^{N-1} \left[\sum_{n=0}^{N-1} w((n-m))_N x(m)\right] W_N^{mk} \\
&= \sum_{m=0}^{N-1} x(m) \sum_{n=0}^{N-1} w((n-m))_N W_N^{mk} \quad (10) \\
&= \sum_{m=0}^{N-1} x(m) \left[\sum_{n=0}^{N-1} w((m-n))_N W_N^{mk}\right]^* \quad (\text{Eq. 7}) \\
&= \sum_{m=0}^{N-1} x(m) W^*(k) W_N^{mk} \quad (\text{Eq. 8}) \\
&= W^*(k) \sum_{m=0}^{N-1} x(m) W_N^{mk} \\
&= W^*(k) \cdot X(k)
\end{aligned}$$

A.2 Theoretical Time Complexity of ParC and Fast-ParC

For simplicity, we compute the multiplication time as FLOPs for the following examples. Considering vanilla 2D convolution with kernel shaped $K_h \times K_w$ and input feature map $H \times W$, every slide include $K_h \times K_w$ times of MUL operation. If using zero-padding to make the output owns the same size as input, the entire map cost HWK_hK_w MUL operations in spatial. Take channel dimension into consideration, we have the following equation:

$$\begin{aligned}
FLOPs(\text{DW-Conv2d}) &= CHWK_hK_w \\
&= \mathcal{O}(CHWK_hK_w) \\
FLOPs(\text{Conv2d}) &= C_i C_o HWK_hK_w \quad (11) \\
&= \mathcal{O}(C_i C_o HWK_hK_w)
\end{aligned}$$

ParC uses positional embedding, global kernel and circular convolution. We use positional embedding by add it to feature map, thus this requires HW ADDs and 0 MULs. Circular convolution could be considered as a different padding scheme, it make no difference in computational complexity comparing with vanilla convolution. ParC use global kernel and 1D decomposition, which means for $C/2$ we use $K_h = H$, $K_w = 1$ and for the other $C/2$ we use $K_h = 1$, $K_w = W$. Reuse Eq. 11, we could know ParC requires MULs of:

$$\begin{aligned}
FLOPs(\text{ParC}) &= \frac{1}{2}CHW(H \cdot 1) + \frac{1}{2}CHW(1 \cdot W) \\
&= \frac{1}{2}CHW(H + W) \\
&= \mathcal{O}(CHW(H + W))
\end{aligned}$$

It's wide acknowledged that FFT facilitate convolution when length N is big. For base-2 FFT with N points, every butterfly transform costs $N/2 \cdot \log N$ MUL operation. And

1D-FFT is completely parallel in the other spatial axis and channel axis. Thus for input map and weight, horizontal 1D-FFT requires $WH/2 \cdot \log_2[H]$ and $H/2 \cdot \log_2[H]$ MULs respectively; and the output requires $WH/2 \cdot \log_2[H]$ for 1D-iFFT. The circular convolution becomes element-wise multiplication of expended weights and input feature map, this requires HW MULs. Since FFT turns real numbers into complex numbers and 1 complex number multiplication equal 4 real number multiplications, the result should be times by 4. Finally, all these operations are parallel in channel axis, hence the result should be times by C :

$$\begin{aligned}
FLOPs(\text{Fast-ParC}) &= \frac{1}{2}C \cdot 4(WH \log_2[H] + \frac{1}{2}H \log_2[H] + HW) \\
&\quad + \frac{1}{2}C \cdot 4(HW \log_2[W] + \frac{1}{2}W \log_2[W] + HW) \\
&= 2CHW(\log_2[H] + \log_2[W]) \\
&\quad + CH \log_2[H] + CW \log_2[W] + 4CHW \\
&= \mathcal{O}(CHW(\log_2[H] + \log_2[W]))
\end{aligned}$$

REFERENCES

- [1] H. Zhang, W. Hu, and X. Wang, "Parc-net: Position aware circular convolution with merits from convnets and transformer," in *European Conference on Computer Vision*, 2022.
- [2] A. Vaswani, N. Shazeer, N. Parmar, J. Uszkoreit, L. Jones, A. N. Gomez, L. Kaiser, and I. Polosukhin, "Attention is all you need," *Advances in neural information processing systems*, vol. 30, 2017.
- [3] A. Dosovitskiy, L. Beyer, A. Kolesnikov, D. Weissenborn, X. Zhai, T. Unterthiner, M. Dehghani, M. Minderer, G. Heigold, S. Gelly *et al.*, "An image is worth 16x16 words: Transformers for image recognition at scale," *arXiv preprint arXiv:2010.11929*, 2020.
- [4] C. Sun, A. Shrivastava, S. Singh, and A. Gupta, "Revisiting unreasonable effectiveness of data in deep learning era," in *Proceedings of the IEEE international conference on computer vision*, 2017, pp. 843–852.
- [5] N. Carion, F. Massa, G. Synnaeve, N. Usunier, A. Kirillov, and S. Zagoruyko, "End-to-end object detection with transformers," in *European conference on computer vision*. Springer, 2020, pp. 213–229.
- [6] Y. Fang, B. Liao, X. Wang, J. Fang, J. Qi, R. Wu, J. Niu, and W. Liu, "You only look at one sequence: Rethinking transformer in vision through object detection," *arXiv preprint arXiv:2106.00666*, 2021.
- [7] S. Zheng, J. Lu, H. Zhao, X. Zhu, Z. Luo, Y. Wang, Y. Fu, J. Feng, T. Xiang, P. H. Torr, and L. Zhang, "Rethinking semantic segmentation from a sequence-to-sequence perspective with transformers," in *2021 IEEE/CVF Conference on Computer Vision and Pattern Recognition (CVPR)*, 2021, pp. 6877–6886.
- [8] F. Z. Zhang, D. Campbell, and S. Gould, "Efficient two-stage detection of human-object interactions with a novel unary-pairwise transformer," in *Proceedings of the IEEE/CVF Conference on Computer Vision and Pattern Recognition (CVPR)*, June 2022, pp. 20 104–20 112.
- [9] A. Ramesh, P. Dhariwal, A. Nichol, C. Chu, and M. Chen, "Hierarchical text-conditional image generation with clip latents," *arXiv preprint arXiv:2204.06125*, 2022.
- [10] J. Guo, K. Han, H. Wu, Y. Tang, X. Chen, Y. Wang, and C. Xu, "Cmt: Convolutional neural networks meet vision transformers," in *Proceedings of the IEEE/CVF Conference on Computer Vision and Pattern Recognition*, 2022, pp. 12 175–12 185.
- [11] S. Mehta and M. Rastegari, "Mobilevit: light-weight, general-purpose, and mobile-friendly vision transformer," *arXiv preprint arXiv:2110.02178*, 2021.
- [12] Y. Chen, X. Dai, D. Chen, M. Liu, X. Dong, L. Yuan, and Z. Liu, "Mobile-former: Bridging mobilenet and transformer," in *Proceedings of the IEEE/CVF Conference on Computer Vision and Pattern Recognition*, 2022, pp. 5270–5279.
- [13] M. Tan and Q. Le, "Efficientnet: Rethinking model scaling for convolutional neural networks," in *International conference on machine learning*. PMLR, 2019, pp. 6105–6114.

- [14] M. Sandler, A. Howard, M. Zhu, A. Zhmoginov, and L.-C. Chen, "Mobilenetv2: Inverted residuals and linear bottlenecks," in *Proceedings of the IEEE conference on computer vision and pattern recognition*, 2018, pp. 4510–4520.
- [15] W. Luo, Y. Li, R. Urtasun, and R. Zemel, "Understanding the effective receptive field in deep convolutional neural networks," 2017. [Online]. Available: <https://arxiv.org/abs/1701.04128>
- [16] X. Ding, X. Zhang, Y. Zhou, J. Han, G. Ding, and J. Sun, "Scaling up your kernels to 31x31: Revisiting large kernel design in cnns," 2022. [Online]. Available: <https://arxiv.org/abs/2203.06717>
- [17] S. Han, H. Mao, and W. J. Dally, "Deep compression: Compressing deep neural networks with pruning, trained quantization and Huffman coding," *arXiv preprint arXiv:1510.00149*, 2015.
- [18] A. Ren, T. Zhang, S. Ye, J. Li, W. Xu, X. Qian, X. Lin, and Y. Wang, "Admm-nn: An algorithm-hardware co-design framework of dnns using alternating direction methods of multipliers," in *Proceedings of the Twenty-Fourth International Conference on Architectural Support for Programming Languages and Operating Systems*, 2019, pp. 925–938.
- [19] X. Liu, J. Pool, S. Han, and W. J. Dally, "Efficient sparse-winograd convolutional neural networks," *arXiv preprint arXiv:1802.06367*, 2018.
- [20] V. Podlozhnyuk, "Fft-based 2d convolution," *NVIDIA white paper*, vol. 32, p. 1, 2007.
- [21] A. Vasudevan, A. Anderson, and D. Gregg, "Parallel multi channel convolution using general matrix multiplication," in *2017 IEEE 28th international conference on application-specific systems, architectures and processors (ASAP)*. IEEE, 2017, pp. 19–24.
- [22] W. Wang, E. Xie, X. Li, D.-P. Fan, K. Song, D. Liang, T. Lu, P. Luo, and L. Shao, "Pyramid vision transformer: A versatile backbone for dense prediction without convolutions," in *Proceedings of the IEEE/CVF International Conference on Computer Vision*, 2021, pp. 568–578.
- [23] Z. Liu, Y. Lin, Y. Cao, H. Hu, Y. Wei, Z. Zhang, S. Lin, and B. Guo, "Swin transformer: Hierarchical vision transformer using shifted windows," in *Proceedings of the IEEE/CVF International Conference on Computer Vision*, 2021, pp. 10012–10022.
- [24] Z. Dai, H. Liu, Q. V. Le, and M. Tan, "Coatnet: Marrying convolution and attention for all data sizes," *Advances in Neural Information Processing Systems*, vol. 34, pp. 3965–3977, 2021.
- [25] B. Graham, A. El-Nouby, H. Touvron, P. Stock, A. Joulin, H. Jégou, and M. Douze, "Levit: a vision transformer in convnet's clothing for faster inference," in *Proceedings of the IEEE/CVF international conference on computer vision*, 2021, pp. 12 259–12 269.
- [26] Y. Li, G. Yuan, Y. Wen, E. Hu, G. Evangelidis, S. Tulyakov, Y. Wang, and J. Ren, "Efficientformer: Vision transformers at mobilenet speed," *arXiv preprint arXiv:2206.01191*, 2022.
- [27] Z. Liu, H. Mao, C.-Y. Wu, C. Feichtenhofer, T. Darrell, and S. Xie, "A convnet for the 2020s," in *Proceedings of the IEEE/CVF Conference on Computer Vision and Pattern Recognition*, 2022, pp. 11 976–11 986.
- [28] K. He, X. Zhang, S. Ren, and J. Sun, "Deep residual learning for image recognition," in *Proceedings of the IEEE conference on computer vision and pattern recognition*, 2016, pp. 770–778.
- [29] R. R. Selvaraju, M. Cogswell, A. Das, R. Vedantam, D. Parikh, and D. Batra, "Grad-cam: Visual explanations from deep networks via gradient-based localization," in *Proceedings of the IEEE international conference on computer vision*, 2017, pp. 618–626.
- [30] D. H. Hubel and T. N. Wiesel, "Receptive fields, binocular interaction and functional architecture in the cat's visual cortex," *The Journal of physiology*, vol. 160, no. 1, p. 106, 1962.
- [31] K. Simonyan and A. Zisserman, "Very deep convolutional networks for large-scale image recognition," *arXiv preprint arXiv:1409.1556*, 2014.
- [32] G. Huang, Z. Liu, L. Van Der Maaten, and K. Q. Weinberger, "Densely connected convolutional networks," in *Proceedings of the IEEE conference on computer vision and pattern recognition*, 2017, pp. 4700–4708.
- [33] A. Araujo, W. Norris, and J. Sim, "Computing receptive fields of convolutional neural networks," *Distill*, 2019. [Online]. Available: <https://distill.pub/2019/computing-receptive-fields>
- [34] H. Le and A. Borji, "What are the receptive, effective receptive, and projective fields of neurons in convolutional neural networks?" *arXiv preprint arXiv:1705.07049*, 2017.
- [35] X. Li, W. Wang, X. Hu, and J. Yang, "Selective kernel networks," in *Proceedings of the IEEE/CVF conference on computer vision and pattern recognition*, 2019, pp. 510–519.
- [36] S. Gao, Z.-Y. Li, Q. Han, M.-M. Cheng, and L. Wang, "Rf-next: Efficient receptive field search for convolutional neural networks," *IEEE Transactions on Pattern Analysis and Machine Intelligence*, 2022.
- [37] H. Touvron, M. Cord, M. Douze, F. Massa, A. Sablayrolles, and H. Jégou, "Training data-efficient image transformers & distillation through attention," in *International Conference on Machine Learning*. PMLR, 2021, pp. 10 347–10 357.
- [38] S. Woo, J. Park, J.-Y. Lee, and I. S. Kweon, "Cbam: Convolutional block attention module," in *Proceedings of the European conference on computer vision (ECCV)*, 2018, pp. 3–19.
- [39] B. Heo, S. Yun, D. Han, S. Chun, J. Choe, and S. J. Oh, "Rethinking spatial dimensions of vision transformers," in *Proceedings of the IEEE/CVF International Conference on Computer Vision*, 2021, pp. 11 936–11 945.
- [40] Z. Huang, X. Wang, L. Huang, C. Huang, Y. Wei, and W. Liu, "Ccnets: Criss-cross attention for semantic segmentation," in *Proceedings of the IEEE/CVF international conference on computer vision*, 2019, pp. 603–612.
- [41] A. Srinivas, T.-Y. Lin, N. Parmar, J. Shlens, P. Abbeel, and A. Vaswani, "Bottleneck transformers for visual recognition," in *Proceedings of the IEEE/CVF conference on computer vision and pattern recognition*, 2021, pp. 16 519–16 529.
- [42] T. Xiao, M. Singh, E. Mintun, T. Darrell, P. Dollár, and R. Girshick, "Early convolutions help transformers see better," *Advances in Neural Information Processing Systems*, vol. 34, pp. 30 392–30 400, 2021.
- [43] S. d'Ascoli, H. Touvron, M. L. Leavitt, A. S. Morcos, G. Biroli, and L. Sagun, "Convit: Improving vision transformers with soft convolutional inductive biases," in *International Conference on Machine Learning*. PMLR, 2021, pp. 2286–2296.
- [44] A. Krizhevsky, I. Sutskever, and G. E. Hinton, "Imagenet classification with deep convolutional neural networks," *Advances in neural information processing systems*, vol. 25, 2012.
- [45] C. Szegedy, W. Liu, Y. Jia, P. Sermanet, S. Reed, D. Anguelov, D. Erhan, V. Vanhoucke, and A. Rabinovich, "Going deeper with convolutions," in *Proceedings of the IEEE conference on computer vision and pattern recognition*, 2015, pp. 1–9.
- [46] S. Liu, T. Chen, X. Chen, X. Chen, Q. Xiao, B. Wu, M. Pechenizkiy, D. Mocanu, and Z. Wang, "More convnets in the 2020s: Scaling up kernels beyond 51x51 using sparsity," *arXiv preprint arXiv:2207.03620*, 2022.
- [47] Y. Rao, W. Zhao, Z. Zhu, J. Lu, and J. Zhou, "Global filter networks for image classification," in *Advances in Neural Information Processing Systems (NeurIPS)*, 2021.
- [48] X. Chu, Z. Tian, B. Zhang, X. Wang, X. Wei, H. Xia, and C. Shen, "Conditional positional encodings for vision transformers," *arXiv preprint arXiv:2102.10882*, 2021.
- [49] W. Yu, M. Luo, P. Zhou, C. Si, Y. Zhou, X. Wang, J. Feng, and S. Yan, "Metaformer is actually what you need for vision," in *Proceedings of the IEEE/CVF Conference on Computer Vision and Pattern Recognition*, 2022, pp. 10 819–10 829.
- [50] C. D. McGillem and G. R. Cooper, *Continuous and discrete signal and system analysis*. Harcourt School, 1991.
- [51] T.-Y. Lin, M. Maire, S. Belongie, J. Hays, P. Perona, D. Ramanan, P. Dollár, and C. L. Zitnick, "Microsoft coco: Common objects in context," in *European conference on computer vision*. Springer, 2014, pp. 740–755.
- [52] B. Zhou, H. Zhao, X. Puig, T. Xiao, S. Fidler, A. Barriuso, and A. Torralba, "Semantic understanding of scenes through the ade20k dataset," *International Journal of Computer Vision*, vol. 127, no. 3, pp. 302–321, 2019.
- [53] J. Li, X. Xia, W. Li, H. Li, X. Wang, X. Xiao, R. Wang, M. Zheng, and X. Pan, "Next-vit: Next generation vision transformer for efficient deployment in realistic industrial scenarios," *arXiv preprint arXiv:2207.05501*, 2022.
- [54] A. Paszke, S. Gross, F. Massa, A. Lerer, J. Bradbury, G. Chanan, T. Killeen, Z. Lin, N. Gimelshein, L. Antiga et al., "Pytorch: An imperative style, high-performance deep learning library," *Advances in neural information processing systems*, vol. 32, 2019.
- [55] C. R. Harris, K. J. Millman, S. J. van der Walt, R. Gommers, P. Virtanen, D. Cournapeau, E. Wieser, J. Taylor, S. Berg, N. J. Smith, R. Kern, M. Picus, S. Hoyer, M. H. van Kerkwijk, M. Brett, A. Haldane, J. Fernández del Río, M. Wiebe, P. Peterson, P. Gérard-Marchant, K. Sheppard, T. Reddy, W. Weckesser, H. Abbasi, C. Gohlke, and T. E. Oliphant, "Array programming with NumPy," *Nature*, vol. 585, p. 357–362, 2020.

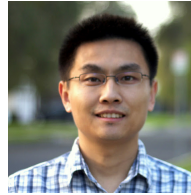
- [56] M. Fatica, "Cuda toolkit and libraries," in *2008 IEEE hot chips 20 symposium (HCS)*. IEEE, 2008, pp. 1–22.
- [57] J. Hu, L. Shen, S. Albanie, G. Sun, and E. Wu, "Squeeze-and-excitation networks," *IEEE Transactions on Pattern Analysis and Machine Intelligence*, vol. 42, no. 8, pp. 2011–2023, 2020.
- [58] S. Woo, J. Park, J.-Y. Lee, and I. S. Kweon, "Cbam: Convolutional block attention module," in *Proceedings of the European conference on computer vision (ECCV)*, 2018, pp. 3–19.
- [59] Y. Li, Y. Chen, X. Dai, D. Chen, M. Liu, L. Yuan, Z. Liu, L. Zhang, and N. Vasconcelos, "Micronet: Improving image recognition with extremely low flops," in *Proceedings of the IEEE/CVF International Conference on Computer Vision*, 2021, pp. 468–477.
- [60] S. Xie, R. Girshick, P. Dollár, Z. Tu, and K. He, "Aggregated residual transformations for deep neural networks," *arXiv preprint arXiv:1611.05431*, 2016.
- [61] I. Loshchilov and F. Hutter, "Decoupled weight decay regularization," *arXiv preprint arXiv:1711.05101*, 2017.
- [62] C. Szegedy, V. Vanhoucke, S. Ioffe, J. Shlens, and Z. Wojna, "Rethinking the inception architecture for computer vision," in *Proceedings of the IEEE conference on computer vision and pattern recognition*, 2016, pp. 2818–2826.
- [63] B. T. Polyak and A. B. Juditsky, "Acceleration of stochastic approximation by averaging," *SIAM journal on control and optimization*, vol. 30, no. 4, pp. 838–855, 1992.
- [64] T.-Y. Lin, M. Maire, S. Belongie, J. Hays, P. Perona, D. Ramanan, P. Dollár, and C. L. Zitnick, "Microsoft coco: Common objects in context," in *European conference on computer vision*. Springer, 2014, pp. 740–755.
- [65] W. Liu, D. Anguelov, D. Erhan, C. Szegedy, S. Reed, C.-Y. Fu, and A. C. Berg, "Ssd: Single shot multibox detector," in *European conference on computer vision*. Springer, 2016, pp. 21–37.
- [66] M. Everingham, S. Eslami, L. Van Gool, C. K. Williams, J. Winn, and A. Zisserman, "The pascal visual object classes challenge: A retrospective," *International journal of computer vision*, vol. 111, no. 1, pp. 98–136, 2015.
- [67] G. Huang, Y. Sun, Z. Liu, D. Sedra, and K. Q. Weinberger, "Deep networks with stochastic depth," in *European conference on computer vision*. Springer, 2016, pp. 646–661.
- [68] Z. Cai and N. Vasconcelos, "Cascade r-cnn: Delving into high quality object detection," in *Proceedings of the IEEE conference on computer vision and pattern recognition*, 2018, pp. 6154–6162.
- [69] K. Chen, J. Wang, J. Pang, Y. Cao, Y. Xiong, X. Li, S. Sun, W. Feng, Z. Liu, J. Xu, Z. Zhang, D. Cheng, C. Zhu, T. Cheng, Q. Zhao, B. Li, X. Lu, R. Zhu, Y. Wu, J. Dai, J. Wang, J. Shi, W. Ouyang, C. C. Loy, and D. Lin, "MMDetection: Open mmlab detection toolbox and benchmark," *arXiv preprint arXiv:1906.07155*, 2019.
- [70] T. Xiao, Y. Liu, B. Zhou, Y. Jiang, and J. Sun, "Unified perceptual parsing for scene understanding," in *Proceedings of the European conference on computer vision (ECCV)*, 2018, pp. 418–434.
- [71] M. Contributors, "MMSegmentation: Openmmlab semantic segmentation toolbox and benchmark," <https://github.com/open-mmlab/mms Segmentation>, 2020.
- [72] K. Z. e. a. Junjie Bai, Fang Lu, "Onnx: Open neural network exchange," *GitHub repository*, 2019.
- [73] X. Jiang, H. Wang, Y. Chen, Z. Wu, L. Wang, B. Zou, Y. Yang, Z. Cui, Y. Cai, T. Yu *et al.*, "Mnn: A universal and efficient inference engine," *Proceedings of Machine Learning and Systems*, vol. 2, pp. 1–13, 2020.



Tao Yang is an undergraduate student at Hon-shen Honers School, Chongqing University. He will receive his B.S. degree in Electronic Engineering in 2023. In 2022, He spent 3 months as an intern at AI Lab, Intellifusion. He is now working as a research assistant at CHEN Lab, The Hong Kong Polytechnic University (PolyU). His research interests include deep learning, computer vision, and model compression.



Haokui Zhang received the Ph.D degree and the MS degree in computer application technology from Shannxi Provincial Key Laboratory of Speech and Image Information Processing in 2021 and 2016. From 2018 to 2020, he spent two years as a Joint-Ph.D with the fund of CSC at AIML Lab, the University of Adelaide. He is currently working as senior algorithm expert at AI Lab of Intellifusion. His research interests cover approximate nearest neighbor search, semantic segmentation, depth estimation, neural architecture search and hyperspectral image classification.



Wenze Hu received a PhD degree from Department of Statistics, University of California, Los Angeles in 2012, and was a postdoctoral scholar at the Center for Vision Cognition Learning and Art in UCLA. He joined Google in August, 2013. He is currently working as technical director at AI Lab of Intellifusion. His research interest include computer vision and statistical modeling.



Changwen Chen received his BS from the University of Science and Technology of China in 1983, MSEE from the University of Southern California in 1986, and Ph.D. from the University of Illinois at Urbana-Champaign in 1992. He is currently Chair Professor of Visual Computing at The Hong Kong Polytechnic University. Before his current position, he served as Dean of the School of Science and Engineering at The Chinese University of Hong Kong, Shenzhen from 2017 to 2020. He also served as an Empire Innovation Professor at the University at Buffalo, the State University of New York from 2008 to 2021. He was Allen Henry Endow Chair Professor at the Florida Institute of Technology from 2003 to 2007. He was on the faculty of Electrical and Computer Engineering at the University of Rochester from 1992 to 1996 and on the faculty of Electrical and Computer Engineering at the University of Missouri-Columbia from 1996 to 2003. His research interests include multimedia communication, multimedia systems, mobile video streaming, Internet of Video Things (IoVT), image/video processing, computer vision, deep learning, multimedia signal processing, and immersive mobile video. He is an IEEE Fellow (2005), a SPIE Fellow (2007), and an elected member of the Academia Europaea (2021).



Xiaoyu Wang received the BE degree from the University of Science and Technology of China, in 2006, the MS degree in statistics from the University of Missouri, Columbia, in 2012, and the PhD degree in electrical and computer engineering from the University of Missouri, Columbia. He is currently chief scientist at Intellifusion. Before joining Intellifusion, he was a founding member of Snap Research and served as chair of computer vision from 2015 to 2017. He was a research scientist at NEC Labs America from

2012-2015. He served as area chair for WACV 2017, CVPR 2022 and CVPR 2023. His team was the runner-up winner of ImageNet Object Recognition Challenge in 2013. His research interests include on Computer Vision and Machine Learning.